SLAC–PUB–95–6489

The Stanford linear accelerator polarized electron source*

R. Alley, H. Aoyagi,[∞] J. Clendenin,[◊] J. Frisch, C. Garden, E. Hoyt, R. Kirby, L. Klaisner, A. Kulikov, R. Miller, G. Mulhollan, C. Prescott, P. Sáez, D. Schultz, H. Tang, J. Turner, K. Witte, M. Woods, A.D. Yeremian, and M. Zolotorev

Stanford Linear Accelerator Center, Stanford University, Stanford, CA 94309, USA

Abstract

The Stanford 3-km linear accelerator at SLAC has operated exclusively since early 1992 using a polarized electron beam for its high-energy physics programs. The polarized electron source now consists of a diode-type gun with a strained-lattice GaAs photocathode DC biased at high voltage and excited with circularly polarized photons generated by a pulsed, Ti:sapphire laser system. The electron polarization at the source is >80%. To date the source has met all the beam requirements of the SLC and fixed target programs with <5% downtime.

1. Introduction

Polarized electron sources have been utilized in physics research for many years and for many purposes. Polarized electrons have been obtained from beta decay of radioactive sources, from polarization-dependent scattering processes, from photoionization of polarized atoms, from photoemission

Submitted to Nuclear Instruments & Methods

---

*Work supported by Department of Energy contract DE–AC03–765F00515.
[∞]Present address: Faculty of Science, Nagoya University, Nagoya, 464–01, Japan.
[◊]Corresponding author email: CLEN@SLAC.Stanford.EDU

from solid materials, and from spin-dependent processes in accelerators. These processes have been put to use in the studies of fundamental properties of the electron, in studies of solids and surfaces, for atomic physics, and in high-energy physics for studies of nuclei, quarks, and gauge bosons. Reviews of the physics and techniques exist throughout the literature [1].

The search for high-intensity, high-brightness sources for accelerators represents one important chapter of the polarized electron story. At the Stanford Linear Accelerator Center (SLAC) in the 1970s, the desire to study the spin structure of the proton stimulated development of a photoionization source matched to the linear accelerator parameters [2]. The photoionization source contributed to several very successful experiments. However the currents from the photoionization process were far below the capability of the SLAC linear accelerator, and experiments requiring much higher currents stimulated the search for new source techniques. In 1974, the development of a cathode material based on gallium arsenide was proposed for a polarized electron source [3]. Combined with existing laser technology, polarization approaching 50% and instantaneous beam currents exceeding one ampere appeared feasible. A polarized source based on photoemission from GaAs was developed for SLAC [4] and operated successfully in 1978 [5]. Subsequently, similar sources were constructed for other electron accelerators, including MIT/Bates, Mainz, and Bonn. During this period, the use of GaAs sources spread to other fields as well.

Developments of the gallium arsenide technology continued into the 1980s. A group at SLAC demonstrated enhanced electron polarization in GaAs through mechanical strain [6]. The advent of the molecular beam epitaxy (MBE) process in industry led to the capability of growing thin epitaxial layers of strained GaAs on wafers of bulk GaAs material. In 1991 a SLAC/Wisconsin/Berkeley group demonstrated high polarization from a MBE-grown cathode of strained InGaAs [7]. Shortly thereafter, high polarization using strained GaAs was achieved [8], [9]. By optimizing the relevant crystal parameters in strained GaAs, an electron polarization above 80% has been achieved in both the laboratory and during use on the SLAC linac for high energy physics experiments.

Linacs are particularly well suited for accelerating polarized electrons since there is no depolarization during the accelerating process. However, incorporating strained GaAs into the high voltage, high vacuum environment needed for reliable, stable accelerator operations was not easy. Development of the gun design, selection and testing of the materials, design of the beam transport optics, development of the cathode handling procedures, and development of an appropriate laser beam took a number of years. With the successful operation of the SLAC Linear Collider (SLC) and several fixed-target experiments at SLAC using polarized beams, the basic principles of gun design for strained GaAs cathodes are well established. In the following sections, we discuss the implementation of these principles for the Stanford linear accelerator.

2. Requirements for SLC and fixed target experiments

The SLC was designed to collide a single bunch of $5x10^{10}$ polarized electrons at the interaction point (IP) with an identical bunch of unpolarized positrons at a center-of-mass (CM) energy of up to 100 GeV [10]. The original 30-GeV, S-band, 3-km linac was upgraded to co-accelerate not only the electron and positron bunches to ~50 GeV each, but also a second "scavenger" electron bunch to ~30 GeV for delivery to a positron production target. The repetition rate of the accelerating rf in the linac can be up to 120 Hz. During acceleration to high energy, the positron bunch leads the electron bunch by ~62 ns, with the scavenger bunch following by yet another 62 ns. The net yield of the positron production system is unity, so that the three microbunches co-accelerated in the linac have equal intensities.

Figure 1(a) illustrates the SLC accelerating system [11]. The two electron bunches are produced by the polarized electron source, bunched and injected at 200 MeV into a 1-GeV S-band linac. The positrons, collected at the positron production target, are transported to the 200-MeV point, then injected with the two electron bunches and co-accelerated to 1.2 GeV. Before injection into the high energy linac, the transverse emittance of the bunches is reduced using damping rings. The two electron bunches are damped for one interpulse period, while the positron bunch, which begins with a much higher emittance, is damped twice as

long. Thus two bunches circulate in each ring when the SLC is operating at 120 Hz. The bunch length and energy spread of the bunches is adjusted during transport from the damping rings to the linac. The relevant beam requirements for the SLC electron source are given in Table 1.

The SLC bunching and injection systems are designed to rapidly compress a 2-ns electron pulse to a few tens of picoseconds while limiting the transverse and longitudinal phase-space growth prior to reaching relativistic energies. Since the polarized source utilizes a photocathode, consideration was given originally to generating a 10-20 ps pulse directly from the gun using an equally short laser pulse [12]. However, it was estimated that the space charge forces for such an intense beam would result in an unacceptable blowup of the beam transverse and longitudinal emittances, well before the beam could be accelerated. It was consequently decided to use the 16th subharmonic of the 2856 MHz accelerating frequency of the linac to bunch a 2-ns gun pulse.

The SLC injector is shown schematically in Fig. 2. The 120 kV electron beam generated at the gun first passes through a vacuum isolation section before beginning the bunching and acceleration process. Two subharmonic buncher (SHB) cavities operating at 178.5 MHz, each with independent phase and amplitude control, are situated in front of a standard SLAC 3-m S-band (2856 MHz) accelerating section modified to have the first four cells function as an S-band buncher. The rf for the S-band buncher, although closely coupled to that for the accelerating section, has independent phase and amplitude control. An electron bunch, after passing through the 2 SHB cavities, enters the S-band buncher with about 100° of S-band phase. The phase-space transformation that takes place in the buncher results in a bunch length of ~50°, after which the length is further reduced to the order of 10° (3 mm) FWHM as the bunch moves toward the crest of the rf during acceleration within the first few centimeters to $\beta > 0.99$.

The design [13] and performance [14] of the SLC injector has been previously described. During 1993, the SLC operated with a damped charge of ~3.0×10^{10} e^- per bunch due to limitations in the damping rings. With the present 2.0-ns FWHM laser pulse, about 80% of the charge from the gun is captured within 18° of

S-band as measured at 200 MeV. Typically, ~80% of this charge is injected into the high energy linac after damping. Since the transmission of the linac to the IP is nearly 100%, the source was required to produce about 5.5×10^{10} e^- per bunch for high energy physics [15]. With recently completed modifications to the damping rings, the intensity at the IP has been raised to the level of 3.5×10^{10} e^- per bunch, which requires $6\text{-}7\times10^{10}$ e^- per bunch at the source.

The fixed-target experiments use the same gun as SLC, but a different laser system, to produce a longer electron pulse with lower peak intensities compatible with polarized nucleon targets. Since the required peak intensities are considerably lower than for SLC, the photocathode can be biased at only 60 kV, which, as will be discussed later, improves the operational characteristics of the gun. At the injector, an S-band prebuncher substitutes for the SHB. Beam pulses of 1–2 μs were accelerated up to ~29 GeV with the linac rf configured for long pulse acceleration, and then transported to the target in End Station A (ESA), bypassing the damping ring. See Fig. 1(b). The ESA beamline is presently being upgraded to 50 GeV for a new set of experiments that will use a shorter (~100 ns) beam pulse.

A description of the performance of the polarized electron source in meeting the requirements of the SLC and the fixed-target program will be given in Section 9, following a detailed description of the source system.

3. Physics of GaAs cathodes

3.1. Negative electron affinity semiconductor photoemitters

For many years direct band gap III-V semiconductors treated to have a negative electron affinity (NEA) surface have been known to be efficient photoemitters into the near infrared regime [16]. For these materials, the band gap is typically about 1.5 eV, while the work function Φ is on the order of 4 eV. In our case, it is convenient to use the effective electron affinity χ defined as the energy difference between the

vacuum and the conduction band minimum in the bulk. When highly p-doped, the Fermi level in the bulk for these materials is normally lowered to near the top of the highest valence band at the Γ point. In the presence of surface states, this results in an accumulation of positive charge at the surface that bends the energy bands downward at the surface by as much as half the band gap, and consequently lowers χ by the same amount. The effective electron affinity may be further lowered by applying Cs and an oxide on the surface until the vacuum level is below the bottom of the lowest conduction band in the bulk, a condition that defines an NEA surface, although the vacuum level remains above the conduction band minimum at the surface.

The technique of activation requires the preparation of an oxide- and carbon-free surface in an ultra-high vacuum system. The clean surface is then coated with an alkali, Cs being the most effective, while monitoring the photoemission with a low-level light source until the photocurrent peaks. A significant further enhancement in yield can be accomplished by additional application of an oxidizer (both O_2 and NF_3 have been used with similar results) at low pressure plus the continued use of the alkali, either alternating the two (the so-called "yo-yo" method) or using co-deposition. The presence of Cs appears to be necessary to dissociate the oxide at the surface [17]. With the application of O_2 and additional Cs, a second higher peak in the yield is achieved corresponding to the formation of a Cs-O layer directly on the substrate. As the activation progresses, the Cs/O ratio drops to ~3 [18]. The fact that the ratio levels off before 2 is an indication of the presence of excess Cs [19] and perhaps also of the formation of Cs suboxides [20].

There are several ways to achieve the clean crystal surface necessary for a successful activation. The most widely used technique in practical electron sources is *in situ* heat cleaning, which will remove all contaminants except carbon. The pre-vacuum cleaning technique, which among other things is designed to minimize carbon, as well as the *in situ* heat cleaning used for the SLC source, is described in Section 7.

The photoemission process in semiconductors is normally described as consisting of three steps: (1) absorption of incident photons in the bulk of the crystal, (2) diffusion of the resulting conduction band electrons to the surface, and (3) emission of electrons from the surface [21]. For uniform photoemitting material, the first two steps are fairly well understood. Absorption of incident photons in the crystal can be described by an optical absorption coefficient $\alpha'(\lambda)$. Since optical absorption measurements have not been made for strained GaAs, the measured values α must be corrected by the relative transition probability $\zeta(\lambda)$ for the states involved; i.e., $\alpha' = \alpha\,\zeta$. For unstrained GaAs, α is fairly flat at ~1 μm^{-1} down to photon energies very near the band gap, at which point there is a precipitous drop. At the band gap of unstrained GaAs at room temperature for a doping of 5×10^{18} cm^{-3}, α is ~0.6 μm^{-1} [22].

The photoexcited electrons rapidly thermalize to the bottom of the conduction band and then either recombine in the bulk or reach the bent-band surface region by diffusion. Using a time-independent diffusion equation, the number of electrons entering the bent-band region per incident photon Y_{int}, can be shown to be simply [23]

$$Y_{int} = (1-R)\,\frac{\alpha' L}{1+\alpha' L}\,[1-\exp\{-(1+\alpha' L)\ (\ell / L)\}]\,, \qquad (1)$$

where R~0.3 is the reflection coefficient for incident photons at the crystal surface, $L = (D\tau_e)^{1/2}$ is the diffusion length, D is the diffusion constant, τ_e is the electron lifetime in the conduction band, and the thickness of the active layer is given by ℓ. For p-type GaAs with a dopant concentration of ~5×10^{18} cm^{-3}, D is ~25 $cm^2\ s^{-1}$ at room temperature and τ_e *is* ~2.7 ns [24]; thus, L is ~2.7 μm. For thick ($\ell >> L$), unstrained ($\zeta = 1$) GaAs, $\alpha' L$ is ~1.6 for excitation near the band gap, and consequently Y_{int}, is on the order of 0.4 at room temperature.

The final yield Y is the product of Y_{int}, and the surface escape probability P:

$$Y = PY_{int}\ . \qquad (2)$$

Measured values of P for GaAs as high as 0.4 have been reported in the literature [25]. It is not surprising therefore to find yields for thick GaAs as high as 15% when the crystal is excited in reflection mode near threshold and >20% at slightly higher excitation energies. However, values of P achieved in practice generally vary over a considerable range that depends on the particular crystal material, the crystal orientation, the dopant and dopant concentration, and most importantly, on the success of the surface preparation. The surface escape probability can be obtained experimentally by measuring Y as a function of α. The mean free path for electron-phonon collisions is on the order of only 5 nm. Since the average energy loss per phonon is about 25 meV at room temperature, for excitation at threshold, most of the electrons arriving at the surface are thermalized. Thus P should be fairly independent of λ, even for cathodes as thin as 0.1 L.

Throughout this paper, the term quantum efficiency (QE), defined as the ratio of the number of photoemitted electrons to the number of incident photons before passing through the vacuum window evaluated at low laser intensities, will be used as a practical measure of the low intensity yield.

3.2. Polarization

A plot of the minority carrier energy E as a function of momentum for bulk GaAs at room temperature is shown in the vicinity of the Γ point at the left of Fig. 3(a). The top of the valence band at Γ_8, as well as the spin-orbit split-off band at Γ_7, has p-type symmetry, whereas the bottom of the conduction band at Γ_6 has s-type. The energy level diagram and transition probabilities are shown in the middle of Fig. 3(a). At Γ_8, the light hole (lh) and heavy hole (hh) bands are degenerate. Under these conditions, if the crystal is illuminated with right (σ+) only or left (σ-) only circularly polarized light, with a photon energy greater than the band gap E_g, but less than E_g plus the spin-orbit energy splitting Δ_{SO}, then electrons excited into the conduction band by σ- light can be expected to have a polarization $P_{\text{int}}^{\sigma-}$ of

$$P_{\text{int}}^{\sigma-} = \frac{N_+ - N_-}{N_+ + N_-} = \frac{3-1}{3+1} = +0.5 \ , \qquad (3)$$

as shown at the right of Fig. 3(a). Here the sign of the polarization indicates the projection of the spin angular momentum along the axis of propagation of the photon. The measured polarization of electrons photoemitted from thick GaAs is generally <50% [26]. Typical values at room temperature are on the order of 30%. At liquid nitrogen (LN_2) temperatures or using thin GaAs, polarizations >40% are typically observed[27].

3.3. Strained lattice cathodes

The success of the SLAC source has been a combination of the reliability of the source over the long operating cycles of the SLC and the fixed-target programs combined with the successful adaptation of strained-lattice GaAs–$GaAs_{1-x}P_x$ cathodes to the source to increase the polarization. The lattice constant of $GaAs_{1-x}P_x$ is smaller than, and can be adjusted relative to, that of GaAs by varying the phosphorus fraction x. If GaAs of the proper thickness is grown on top of the $GaAs_{1-x}P_x$ sublayer, the resulting bi-axial compressive strain (uni-axial tensile strain along the growth direction) within the GaAs layer will lift the degeneracy of the lh and hh bands [9], [28] at Γ as shown in Fig. 3(b) [29]. Note that if the hh band is energetically higher than the lh band, as is the case for bi-axial compressive strain, then the resulting electron polarization has the same sign as for bulk GaAs if the excitation light has the same circular polarization sign. If the band splitting δ is larger than the rms variation in the energy band tailing due to the high doping concentration [30], then in principle it should be possible to achieve 100% polarization using circularly polarized light with photon energy between E_g and $(E_g+\delta)$.

3.4. Space charge limit and cathode charge limit

It is well known that for an electron gun, space charge limits the maximum current that can be extracted from the cathode. By Child's law, this current varies as $V^{3/2}$ where V is the extraction voltage across the cathode-anode structure. An additional limitation on the total charge that can be extracted in a short time period applies to semiconductor photocathodes [31]. This internal charge limit has been thoroughly explored at SLAC for nanosecond-long excitation pulses (some complementary data is available for microsecond-long pulses). The principle finding, which is essential for the SLC, is that the maximum charge (or conversely, the limitation on the charge) in a 2–ns pulse that can be extracted from a GaAs-type cathode, whether or not it is strained, is essentially independent of the thickness of the active layer. The characteristics of the cathode charge limit as it affects the performance of the SLC source will be discussed in Section 9.1.

4. The polarized electron gun

4.1. Gun design

The gun follows the conventional design for thermionic-cathode guns in which a cathode at high voltage (HV) is supported by a large ceramic insulator. This insulator forms a major portion of the vacuum wall [32]. The incident laser beam and the resulting electron beam pass through a hole in the center of the grounded anode. A cross section of the gun is shown in Fig. 4.

To minimize the space charge forces that can severely disrupt the electron beam while it is still non-relativistic, the beam energy must be as high as possible while maintaining the minimum gradient at the cathode sufficient to extract the required charge. The diode electrode design adopted for this purpose is similar to that used in a grided thermionic gun [33] that was successfully employed during the commissioning of the SLC injector [34] to produce 2-ns pulses with the charge required for the SLC [14]. A triode photocathode gun [35] designed and built at SLAC in the early 1980s was never implemented for the SLC. With the present SLC photocathode gun design, the anode is separated from the cathode by about 3

cm. There is no intermediate electrode as in the triode gun design. The field gradient at the photocathode surface is calculated using EGUN [36] to be 1.8 MV/m at 120 kV. The zero-charge field potentials are shown in Fig. 5. The space-charge limit of the gun for a bias of 120 kV is about 15 A for illumination of the full active area (a circular area of diameter 20 mm) of the photocathode [37]. The normalized gun emittance at the space-charge limit calculated by EGUN for the 20 mm cathode biased at 120 kV is 35 mm-mrad.

Vacuum and high voltage performance are the two key issues for the polarized electron gun. An ultrahigh vacuum (UHV) is essential for an activated NEA photocathode to survive in the gun with a reasonably long lifetime. Equally important, the gun must be able to hold off the required voltage with minimal dark currents. The design of the gun is centered around two goals that must be achieved simultaneously with operation of high current beams: (1) a vacuum of $\leq 1x10^{-11}$ Torr in the gun chamber with minimum presence of oxidizing gas species (e.g., H_2O, O_2, and CO_2), and (2) a dark current of <50 nA at the operating voltage.

4.2. High voltage electrode design

The cathode electrode is supported on the end of a 10-cm diameter stainless steel cathode support tube. The photocathode is mounted on a molybdenum puck (see Section 6.3) which is attached to the end of a 3-cm diameter stainless-steel emitter tube. The cathode end of the emitter tube is made of Mo to be compatible with the requirement for high-temperature heat cleaning of the photocathode in a UHV environment. In normal operation, the emitter tube is inserted inside and concentric to the cathode support tube such that the photocathode active surface is exposed to the electric field through a 20-mm diameter hole in the center of the cathode electrode [38]. A more extensive discussion of the operation of the emitter tube is found in Section 6.2.

The components just described are mounted on one end of the cylindrical alumina insulator. The cathode support tube is inside and concentric with the insulator. The other end of the insulator is mounted to the grounded body of the gun vacuum vessel. The HV insulating ceramic is 39.5-cm long with an inner diameter of 19.0 cm and a fluted outer surface [39].

The anode electrode is mounted to the anode support tube which is attached to the grounded portion of the gun vacuum chamber. Large holes in the anode support tube improve vacuum conductance from the pumps to the volume in front of the active photocathode. The anode and cathode electrodes were designed to reduce the maximum field strength on the cathode electrode surface. This is important since the high-electric-field region on the electrode surface is the principle source of field emission. At a cathode potential of 120 kV, the highest field on the electrode surface is 7 MV/m at a radius of ~6.5 cm.

The anode and cathode support tubes are attached to the gun body using custom-sized spacing shims (three each). The thickness of the shims is determined during assembly to 25 μm using an alignment fixture. The fixture also locates the anode and cathode radially with a precision of 100 μm. The alignment fixture is precisely mounted to the large, 56-cm diameter flange on the gun body. In this way the electrodes are aligned with respect to each other and to an external reference with the accuracy given.

The anode and cathode electrodes were fabricated using 317L stainless steel [40]. This material was chosen for use in the highest field regions because it had been manufactured with particular care for cleanliness which resulted in a very low carbon content and low inclusion density. The cathode support cylinder and anode support tubes were machined from 304L stainless steel forgings.

Great care was taken in the fabrication of the electrodes, with zero tolerance for visible pits or scratches, to ensure satisfactory high voltage performance [41]. After the electrodes were machined using UHV procedures, they were chemically cleaned and hydrogen fired to 1050 °C for 10 minutes. They were then polished with diamond paste to a 1-μm finish. The material was again chemically cleaned, then

inspected and vacuum fired. All surface areas of the electrodes were finally inspected under a microscope just prior to assembly. Any visible evidence of pitting or surface irregularity caused the part to be returned for further polishing and chemical cleaning. Extreme cleanliness was emphasized throughout the process. Teflon fixtures were used for holding components during transport and extensive care was taken to prevent any contact with polished surfaces. The assembly and alignment of the electrode structure of the gun was done in a Class 100 clean room by fully suited personnel in order to minimize contamination and improve high voltage performance.

4.3. Ultrahigh vacuum

The materials used in the construction of the gun were chosen for UHV compatibility. Components not already mentioned in the previous section include the vacuum housing and ports, which were made from seamless 304L stainless steel tubing, as were the standard flanges. After UHV chemical cleaning, all parts were degassed prior to assembly by vacuum firing at 450°C until the pressure showed no change over at least a 24-hour period (usually ~2 days).

The gun has two main system pumps: a Perkin Elmer 120 differential ion (DI) pump and an SAES Getters Mk 200 non-evaporable getter (NEG) pump. To minimize the stray magnetic field at the photocathode, the ion pump is mounted well away from the gun as shown in Fig. 6. Both pumps have excellent conductance to the photocathode [42].

To obtain the best vacuum conditions, all parts of the gun are designed to be baked at high temperature. The gun assembly, without LoadLock (see Section 6) and before attachment to the beamline, is baked in an oven using circulating hot air. The temperature is controlled by a microprocessor which can also be programmed for a variety of temperature profiles. The temperature of the bakeout is limited to ≤250°C by material in the magnetic lens which is captured on the beam pipe immediately downstream of the gun. The ramp up to full temperature is usually done at a rate of 25°C/hour for the final 100 degrees to minimize

differential expansion of the HV insulator. The bake at high temperature continues until the pressure no longer is significantly dropping, typically ~100 hours, with the pumping done by a dedicated external ion pump. The channel cesiators are cycled during this period. At the end of the 100-hour bake, the NEG pump is processed [43], after which the temperature is ramped down to 150°C to continue the pumping of dissolved gases from surfaces while halting the evolution from the material interiors. During the 8 hours that the temperature is maintained steady at 150°C, the main system pump is turned on and the bake pump is isolated from the system. The system is finally cooled to room temperature and is then ready for installation. Note that neither the emitter tube nor the photocathode are in the gun vacuum chamber during this bake.

A VG Quadrupole residual gas analyzer (RGA) is mounted on the gun vacuum chamber near the cathode. When the gun is in use on the accelerator, the partial pressures of several gas species are recorded every 6 minutes by the SLC computer control system. The RGA is also used to diagnose problems as they arise, and is an extremely sensitive diagnostic for leak checking. The total pressure in the SLC gun during accelerator operations (with rf on) as measured by the gun RGA is typically ~10^{-11} Torr, dominated by H_2 [44], with the partial pressures of CO~2×10^{-12} and $CO_2<1\times10^{-14}$ Torr as shown in Table 2 [45]. The spectrum is unaffected by the presence of the beam or by the HV if the dark current is <100 nA.

4.4. Vacuum isolation of gun

Optimal performance of an activated NEA cathode requires an ultrahigh vacuum on the order of 10^{-11} Torr in the gun. While such a vacuum is readily attained in an isolated gun vacuum volume when high pumping speeds are present, the challenge is to maintain such an ultrahigh vacuum when the gun is open to the accelerator injector where the vacuum is typically several orders of magnitude worse. Therefore, the ultrahigh vacuum in the gun must be decoupled from the higher pressures downstream in the injector. This is achieved by incorporating a vacuum isolation section between the gun and the SHB [46]. The isolation section is equipped with an SAES Getters Mk 500 NEG pump closely coupled to the

beamline and a Perkin Elmer 220 DI pump. The latter, along with another VG RGA, can be isolated with a large gate valve. A 38° bend located immediately downstream provides additional isolation. The net result is that when the gun isolation valve is closed after a period of accelerator operations, the only changes seen in the RGA spectrum given in Table 2 is that the mass-4 peak drops to zero and the mass-28 peak drops by about 30%. The accelerator vacuum has been observed to have some deleterious effect on the cathode lifetime, at least when the operating lifetime is already fairly high (≥500 hour).

The isolation section also facilitates the installation or exchange of guns. A gun is prepared for high vacuum and tested in the laboratory, vacuum sealed with an inline isolation valve, then transported to the injector. Likewise, the downstream end of the vacuum isolation section is equipped with an inline isolation valve. Changing a gun requires venting only the isolation section, which, owing to its high pumping capacity, can be rapidly restored to UHV with a short bake [47]. The entire gun-exchange process—including restoration of vacuum to the isolation section, re-installation of the cathode loading system, cathode activation, and purging of the outer containment vessel—takes about 3 days.

4.5. Electron optics

In order to meet the high intensity requirements of the SLC, the gun was originally designed to operate at 150 kV so that the space charge limit would not become a limiting factor in the beam intensity. During early testing, it was found that 150 kV was too high for reliable operation with an activated NEA cathode. To improve reliability, the gun has been operated for SLC with a cathode bias of 120 kV. This voltage has been sufficient for the beam intensities required by SLC in the past. The original 14-mm cathode diameter and the corresponding anode aperture have been enlarged to improve the charge performance of the gun while still operating at 120 kV.

High efficiency of beam transmission from the gun to the injector is essential, since minor beam interception close to the photocathode may significantly degrade the NEA surface due to electron-

stimulated gas desorption. The basic electron optics design was calculated using the EGUN code to model the gun electrode structure and the CONDOR electromagnetic simulation code to model the transport line [48]. In Fig. 2, the beamline up to the SHB cavities has an inner diameter of ~3.5 cm except for a constriction of 2.5 cm at the 38° bend. Since space-charge forces become important for high intensity beams at 120 keV, a series of iron-encased solenoidal magnetic lenses and a pair of air-core Helmholtz coils are used to generate appropriate axial fields along the beam line to control the transverse beam size. The beam size is made to vary gently over the entire length of the vacuum isolation section by using a smooth, slowly-varying field provided by a pair of Helmholtz coils. Three thin magnetic lenses, located immediately after the gun anode, and before and after the 38° bend, provide localized fields that serve to focus the beam through the first valve and also through the 38° bend chamber. A bucking coil, which is wound around the first lens, is used to zero the magnetic field at the cathode so that the beam emittance is minimized. Both the first lens and the bucking coil are water cooled to prevent heating up the vacuum chamber near the cathode, which might degrade the gun vacuum and thus the cathode performance. More air-core solenoids are used to control the transverse beam size throughout the first and second SHB region, the S-band buncher, and the first 3-meter accelerating section. At this point the beam reaches an energy of 40 MeV and space-charge forces are no longer important.

To help in tuning the injector for high-charge transport, PARMELA, a three-dimensional ray-tracing code with a two-dimensional space charge model, was used to simulate beam transport from the gun through the first accelerating section [49]. The magnetic field profile due to the optics was calculated using POISSON, while SUPERFISH was used to calculate the space harmonics of the various bunchers and the accelerator cavities. The initial beam conditions in the PARMELA code were derived from the EGUN simulation of the gun. The resulting injector parameters from the PARMELA simulation were used to provide initial settings for the injector components which were then optimized experimentally. Beam loss downstream of the gun to the end of the SHB region is monitored by photomultiplier tubes (PMTs)--sensitive enough to detect beam losses of ~1×10^8 electrons. These PMTs are strategically placed along the beam line. Magnetic dipole correctors along with stripline beam position monitors are used to minimize

beam loss and simultaneously to optimize the beam orbit. Additional devices used to tune or characterize the beam in the injector consist of fast wall-gap current monitors, a wire scanner profile monitor, and (not shown in Fig.2) a bunching monitor and an energy analyzer.

Electrons magnetically reflected by the SHB solenoid, as well as backward accelerated electrons from the injector accelerating section, can be seen with the PMTs displaced in time from the initial bunch. The former can be minimized with orbit corrections made with the S-band rf turned off. Reverse direction electrons are in any case bent away from the cathode by the 38° bend shown in Fig. 2.

5. Dark currents and high-voltage processing

Dark current is caused by field emission from metal surfaces. Field emission occurs when the electric fields are high enough to lower the metal surface potential barrier sufficiently for electrons to tunnel out [50]. The local electric field can be enhanced several orders of magnitude by the presence of irregularities on the electrode surfaces, including the presence of semiconducting particles [51] such as dust. Dark currents adversely affect the gun vacuum by stimulated gas desorption and may also permanently harm the cathode by ion bombardment of the photocathode surface. Dark currents have been seen to degrade the lifetime and to irreversibly reduce the QE of the photocathode at a level as low as 100 nA.

In order to maintain a good vacuum and achieve a low dark current, it is necessary to thoroughly process the photocathode gun at high voltage. In previous iterations of polarized guns at SLAC, each gun was baked with its cathode in place and HV processed to eliminate field emission sites. This initial processing inevitably resulted in a cathode surface that could not be successfully activated. The gun was then vented using nitrogen gas, and the final cathode installed. Since the gun had been vented, it was re-baked, which then often required additional HV processing with its concomitant potential for cathode damage [52]. The loss of QE following a HV discharge was often not fully recoverable [53]. The only way to break this cycle was to introduce the final photocathode after the HV processing, but without breaking

vacuum. The apparatus for installing and removing cathodes in this gun without breaking vacuum is described in Section 6. For the field gradients employed in this gun, a newly introduced cathode does not require additional HV processing.

The field-emitted electrons in the gun are accelerated to the grounded surfaces where they desorb gases and generate x-rays. X-ray-sensitive photographic film [54] was used to map the x-ray emitting spots inside the gun. X-rays going through a small aperture on a lead-plate fiducial external to the gun cast an image on film arranged around the electrode area. Multiple small spots on the film indicated that the field emitting sources were discrete point sources. Ray tracing analysis showed that most field emitting points came from the cathode electrode and the cathode support tube. This conclusion was confirmed by the pitting pattern viewed under a microscope and analyzed using a energy dispersive x-ray spectrometer for surface samples taken from a gun after HV processing.

The procedure used for HV processing a gun was intentionally conservative. Since the x-ray intensity increases in proportion to the dark current, the dark current was kept <20 μA to prevent permanent damage to the electrode structure. The main diagnostics used during processing were the cathode nanoammeter (see Section 7.3), a portable x-ray detector, and an RGA. A resister of ~20 MΩ was sometimes used in series with the HV power supply to limit the energy in a HV discharge.

The procedure was to raise the voltage slowly to 60 kV. Typically only minor discharges (spikes in the current together with small, short bursts of CO, H_2, and other gases) were observed. Above ~60 kV the guns typically started drawing 1–20 μA of current. Constant voltage was maintained until the current decreased, which could occur gradually or would sometimes suddenly drop following a HV discharge. This processing could be considerably accelerated by introducing N_2 [55] in the range of 10^{-7}–10^{-6} Torr. To attain a dark current of <50 nA at the operating voltage of 120 kV, the guns were processed in this manner up to 140–180 kV. The rate of raising the voltage varied, taking from a few hours to more than a week.

6. LoadLock

6.1. Necessity for a system to load cathodes into and remove them from the gun chamber under vacuum

The principle benefit of installing the photocathode crystal into the gun without breaking vacuum was to permit the cathode to be installed after processing the gun for high voltage, as discussed in Section 5.

A second benefit (and the original motivation) was to avoid the cathode contamination that normally accompanies the bake of the gun vacuum system [56]. In fact, using normal heat cleaning (HC) methods to activate the cathode, the initial QE following a bake of the cathode with the gun is typically a factor of about 2 lower than routinely achieved with a vacuum loading system [57].

Finally, a vacuum-loading system provides a much more rapid and reliable way to exchange photocathode crystals than is possible by the venting-baking method. The operational advantage of such a system for a large accelerator is obvious.

The vacuum system for loading cathodes developed for the gun is herein called LoadLock . It consists of a motion device that holds the cathode, an isolation valve and ion pump, a cathode activation station, and a cathode storage and exchange system [58]. LoadLock is described below.

6.2. LoadLock functional features

This section describes the mechanical, materials, and operational aspects that make LoadLock unique. Figure 7 is a cutaway view of the mechanical components. The cathode is mounted on the Mo puck described in Section 6.3. The puck couples onto the end of the emitter tube and is held tightly by a pair of

sapphire rollers tensioned by Mo leaf springs. The tube structure of the emitter assembly is necessary to allow heating or cooling of the cathode. Cooling of the cathode is described in Section 7.3.

The use of a tube for supporting the cathode crystal requires the use of a very long bellows to translate the tube from a cathode position in the LoadLock chamber to the operating position in the gun and vice-versa. To accomplish precise translation of the tube over this 1–m distance, a special transport system must be temporarily installed at the LoadLock. The gas vessel and corona shield described in Section 6.4 must first be removed; then a pair of rails is installed under the LoadLock. A plate which moves along the rails is then attached to the rear (upstream) end of the emitter tube. This plate may be adjusted for tilt in orthogonal directions to correct for gravitational forces on the tube and for other minor misalignments in order to accurately dock the puck in the gun cathode electrode. At the rear of the cathode electrode is a guide cone or "dock," shown in Fig. 8, which simplifies engagement. The cone is made of alumina to avoid welding, although the accumulation of some alumina chips during repeated operation is unavoidable.

For heat cleaning the cathode as part of the activation process, the gun HV is first reduced to zero, the gas vessel and corona shield surrounding LoadLock are removed, and the emitter tube (described below) is then extracted from the gun into LoadLock. A nitrogen-gas heater unit with a resistance heater at the cathode end is then inserted into the emitter tube. Gas is forced through the hot zone and subsequently exits out the tube to the atmosphere. The sapphire rollers on the leaf springs grip the sides of the puck without the danger of welding or heat loss during the heating process.

Cold and hot welding of mating surfaces in the LoadLock has been eliminated by using dissimilar metals or insulators. The exception is the end of the emitter tube (Mo) which fits into the back of the puck (Mo) with a clearance around the plug circumference of 0.1 mm on the diameter. No occurrence of welding has been observed.

A tray holds three cathodes and a heating reflector (described in Section 7.2). The tray is in a small vacuum chamber with its own isolation valve to the LoadLock so that trays may be exchanged without bringing the LoadLock up to atmosphere.

The transfer of a cathode from the tray to the emitter tube is accomplished using a pair of vertically mounted Ti rods (the "cathode transfer fork" shown in Fig. 7) as follows. The tray is moved horizontally until the desired puck is over the fork. The fork is then moved upward and slid into grooves on the puck sides. Moving the tray transversely, the fork snaps the puck off the tray. Fork and puck are then lowered, the tray moved out of the way, and the fork moved vertically upward to the emitter tube level where the process is reversed. Guides attached to the chamber wall support the fork during the transverse stress of the snapping procedure.

6.3. Materials and processes

Because of the extreme sensitivity of the photocathode surface to some carbon-containing residual gases, it was essential to use only low-outgassing materials that had been thoroughly degassed at elevated temperatures prior to their use in LoadLock. Brazing of parts was used to eliminate crevices that could act as virtual leak sources. The bellows have a large surface area and are not recleanable for applications as stringent as this, so the segments were cleaned prior to being welded into the bellows, and the completed assemblies were then vacuum-fired to 550°C. The flanges were welded afterwards to avoid softening of the knife edges. Materials used in LoadLock were Ti, Mo, Cu, stainless steel, high-density alumina ceramic, and sapphire. Large clearances and proper design eliminated lubricant use on bearings. During LoadLock qualification testing, residual gas analysis showed 99.9% H_2 at a total system pressure of 3×10^{-11} Torr. During heating of a new cathode, the pressure may rise into the high 10^{-8} Torr range, but this gas is >99% H_2; (the H_2 might even be beneficial in removing oxides and hydrocarbons from the GaAs surface at 600°C) [59].

The GaAs photocathode material is a 650-μm-thick crystal and is very prone to fracture. The crystal must be held in the gun in such a way that stress on the crystal is small. Prior to insertion into the LoadLock vacuum, the GaAs crystal is mounted on a molybdenum puck as shown in Fig. 8. The GaAs disk is set into a shallow depression in the Mo to restrain it from lateral motion. A tantalum cap ring is placed over the GaAs and the side of the puck. A 250-g weight aided by additional hand pressure holds the Ta cap against the GaAs while its bottom edge is crimped around the Mo piece. This assembly holds the GaAs to the puck for LoadLock transfers, heat cleaning, and for placement into the gun.

The emitter tube to which the GaAs wafer and puck are attached is connected to the high-voltage end of the gun with a vacuum bellows. This places a 20-lb force on the emitter tube which must be restrained by the back side of the stainless steel cathode electrode. Six fingers machined into the puck surrounding the GaAs wafer hold the puck against the cathode electrode so the photocathode itself is free of stress. These fingers also position the puck laterally by fitting precisely into an alumina guide cone or dock mounted on the back of the cathode electrode. The dimensions of the puck and Ta cap are tightly controlled to provide a net clearance of ~0.1 mm between the crystal and the cathode electrode in order to avoid crushing and possibly breaking the crystal when initially seating it.

6.4. Operation at high voltage

The use of a mechanically-coupled emitter tube required that LoadLock operate at the gun high voltage. Both the gun parts at HV and LoadLock were enclosed in a polished aluminum corona shield. The exposed eyelets of the ceramic insulator were also covered with spun aluminum corona shields. The corona shield assembly and the ceramic insulator were all enclosed in a large grounded aluminum vessel that was attached to the 56-cm diameter flange on the gun body. A dielectric gas, such as SF_6 or dry air, can be used to fill the large vessel to hold off the high voltage externally; i.e., outside of the gun vacuum. With SF_6, satisfactory performance at 120 kV was typically achieved in a few hours. The moisture level inside the large gas vessel was minimized by circulating the gas through a desiccator to ensure optimal

external high voltage hold-off. Because of safety concerns about asphyxiation danger in the confined space of the accelerator tunnel, SF_6 was only used temporarily when this large volume was first closed. Once satisfactory external high voltage performance was obtained, dry air was circulated instead of SF_6. Dry air is also free from the danger of toxic compound formation that can occur from sparking in SF_6 [60]. The switch over to dry air was normally done after 8-12 hours.

7. Processing cathodes

7.1. Storage and preparation

The photocathode material reported on in this paper consisted of vertical gradient freeze (VGF) [61] grown GaAs [62], molecular beam epitaxy (MBE) grown AlGaAs [63], and metal organic chemical vapor deposition (MOCVD) grown strained-lattice GaAs [64] prepared as 5-cm diameter round wafers [65]. The AlGaAs material was manufactured with a thin As protective coating. The layer structure of the 100-nm strained-lattice cathodes, shown in Fig. 9, followed the prescription of sample (3) in Ref. [9]. Upon receipt, the active surface of a strained-layer wafer was immediately anodized [66]. To protect surfaces from further contamination, wafers were adhered to glass slides [67] with household paraffin for protection; the glass also served as a support for the cutting process. Cathodes were stored at room temperature in a box pressurized with dry N_2 by bleed–off from an LN_2 storage tank. Circular cathodes were cut from wafers using an ethanol and water-irrigated 0.2-mm diameter diamond wire saw at a feed rate not exceeding 14 cm/hour. Material too small for use as a cathode was used to characterize the wafer in the Cathode Test Laboratory prior to employing a cathode from the same wafer in the gun.

Cathodes were prepared for use by first removing the paraffin bonding them to their glass supports with boiling trichloroethane [68]. If anodized, the oxide layer was then stripped off using NH_4OH followed by deionized H_2O and methanol rinses and filtered N_2 drying [69]. Vertical gradient freeze GaAs was etched in a 4:1:1 solution of H_2SO_4, H_2O_2, and H_2O, and then rinsed in H_2O and methanol followed by N_2 drying

[70]. A final rinse in methanol and blow dry with 1-μm filtered N_2 was performed just prior to mounting a cathode in a Mo puck.

Cathodes were mounted on pucks immediately after the final cleaning treatment and then loaded into the puck tray (see Section 6 for a complete description). The tray was attached to the LoadLock volume where it was put under vacuum within 30 minutes. The cathode tray was subsequently baked at 250°C for 4 hours. After cooling, the all metal-seal gate valve separating the puck tray from the LoadLock volume proper was opened so that a puck may be moved to the emitter tube for cathode activation.

7.2. Heat cleaning behavior

Several characteristics of GaAs and LoadLock made heat cleaning to 600°C difficult but attainable. The snap-on puck design, which was essential for cathode exchange, resulted in a significant thermal drop between puck and emitter tube plug end. Added to the drop between the wafer and the puck, the total resulted in a 200°C difference between the GaAs surface and the air side of the tube. The Mo end of the tube was attached to the flanged stainless tube via a Kovar transition piece. This assembly incorporated high temperature cleaning, Ni-plating, and diffusion bonding of the Kovar prior to final braze to eliminate the oxide layer that can form on the Kovar surface [71].

Heating cathodes was also severely hampered by the high emissivity of GaAs (0.7 at 1.06 μm. spectral at 600°C). A number of measures were incorporated into LoadLock to compensate for these problems.

- For the small diameter (18 mm) cathodes used originally in the polarized gun, it was sufficient (1) to electropolish the Mo pucks to reduce their emissivity and heat loss; and (2) to increase the puck-to-plug-end pressure by pushing against the puck face during heating, using the transfer fork. This fork has alumina inserts at the point-of-puck contact to eliminate hot welding. Temperature scans of the wafer face during heating with a GaAs-optimized pyrometer [72] showed a uniform surface temperature at 600°C.

- With the present (22.5 mm diameter) cathodes, the center of the wafer was more than 50 C° cooler that the edges due to radiation loss. In fact, the wafer edge under the Ta clamp ring could rise above the congruent evaporation point while the center was below 600°C. The Ta clamp ring acted as a radiation reflector in that area. That observation was the motivation to add a polished, curved Ti reflector sheet that could be positioned with the fork to ~1 mm in front of the crystal during heating. The reflector occupied a puck position on the tray when not in use. By using this reflector, the larger cathodes could be heated uniformly to the desired temperature.

Following several heating cycles, the reflector sheet showed evidence of GaAs deposition. Using x-ray photoelectron spectroscopy (XPS), the stoichiometry and thickness of this layer was measured to calibrate the loss-per-heating from the cathode surface. The XPS results showed that for a chemically-etched VGF GaAs wafer, the layer had a Ga/As ratio of one. The vapor pressure curves for Ga and As in GaAs as a function of temperature show why this result is not suprising: at 600°C, the atomic rates are about equal [73]. A thin stressed layer of GaAs, therefore, should not become disproportionate due to heat cleaning at 600°C. The measured film thickness on the reflector sheet corresponded to a 7.5-nm lost thickness per 1-hour heating cycle.

7.3. Activation, monitoring, and recesiation

The activation process consisted of first heat cleaning the cathode to 600°C for 1 hour. After the cathode had cooled to room temperature [74], an NEA surface was prepared by deposition of Cs and then NF_3. First, Cs from an effusion cell source [75] was applied. Upon reaching a peak in the QE (measured using a white light source and, subsequently, a HeNe laser), NF_3 was administered at a pressure of $\sim 10^{-9}$ Torr via a leak valve until a new, higher peak was attained. The NF_3 flow was adjusted to keep the yield rising at a reasonable rate. The application of NF_3 resulted in an increase in the electron yield of more than an order of magnitude. After a second peak in the yield was achieved, the NF_3 source was closed off; the Cs source was left on until the yield had diminished by ~10%. This over-cesiation process resulted in a

longer effective lifetime for the cathode. Upon termination of the activation, the photocathode was immediately moved into the gun vacuum volume where it was seated on the rear side of the cathode electrode.

The performance of the gun was monitored using two nanoammeters [76]. The cathode nanoammeter was mounted within the corona shield of the gun, and so measured only the beam current drawn from the photocathode, the dark current from the cathode structure, and the leakage current along the ceramic insulator. A second nanoammeter (the gun nanoammeter) was installed between the high-voltage supply and the gun, where it was used to measure the total current entering the gun structure. This current included the leakage from the corona shield, and the leakage along the cable or along the G-10 [77] supporting LoadLock, in addition to the cathode current. Both nanoammeters were at high voltage during gun operation, and so were powered and read out through fiber-optic links. The output of the nanoammeters was monitored through the SLC computer control program.

The QE of the photocathode was continuously monitored during accelerator operations. For the 100-nm strained-lattice cathodes, an 833-nm continuous-wave (CW) diode laser was mounted on a side window of the gun vessel and was directed, via a pair of polished stainless steel mirrors, to the photocathode. The light from the diode laser was modulated at 1.5 Hz with a 50% duty cycle. The small (about 100 nA), modulated photocurrent from the low-power illumination was sensed with the cathode nanoammeter. A lock-in amplifier was used to continuously measure the modulated current during normal SLC operation when the total DC current was on the order of several microamperes. Since the power of the diode laser was constant (and separately monitored), the lock-in amplifier output could be calibrated in units of QE. The measured value of the QE was recorded every 6 minutes by the SLC computer control program. Monitoring the QE during SLC operations helps characterize the cathode performance to determine when it will become necessary to restore the QE by depositing additional Cs on the surface of the photocathode.

Cesium channel dispensers, made by SAES Getters, were mounted just behind the anode electrode [78]. Four dispensers [79] were mounted on a retractable flange downstream of the anode electrode in a square pattern, with each channel generally directed at the photocathode through the anode hole. In practice the cesiator channels were never retracted and the electron beam simply passed through the center of the assembly. For cathode recesiation in the gun chamber, the high-power pulsed laser was blocked and the high voltage reduced to 1 kV. The cesiator current was then turned on, while the change in photocurrent during the cesiation process was monitored using the cathode nanoammeter [80]. A software program was used to perform these operations in a predetermined pattern initiated by a single command. The whole process took about 15 minutes, dominated by the purposely-slow ramp-up (about 20 kV/minute) of the HV power supply.

Provision was made for cesiating while the beam was running—either continuously [81] or discretely—without turning down the voltage. This consisted of a supply to bias the channels negative so cesium ions would not be emitted. In addition, the cesiator heater current could be turned off during the beam pulse to eliminate any steering effects on the beam. The cathode has been successfully cesiated at 120 kV in the laboratory with the beam off. However, tests of any possible long-term effects on the cathode have not yet been made.

During normal operation, the source temperature was held to a constant value by circulating temperature-controlled N_2 gas down the inside diameter (atmosphere side) of the emitter tube. Since the entire LoadLock was at HV, the gas was brought to the emitter tube through Teflon tubing [82]. The cathode was cooled by thermal conduction through the thin tube end to the puck. Laboratory measurements with a bulk GaAs cathode in a gun operating at 120 kV indicated that significant improvements in QE lifetime could be achieved by operating the cathode below room temperature [83]. Consequently, the cathode temperature was consistently regulated at 0°C. It is noted that in the vacuum system of the SLAC guns, there is little evidence of significant condensation of residual gases on a cathode operated at 0°C [84].

8. Polarized light source

8.1. Laser development at SLAC

When the polarized source was initially operated for the 1992 SLC run, a flashlamp-pumped dye laser (a modified commercial unit) was used as the light source [85]. When development of this laser system began at SLAC, tunable solid state materials were not widely available. The operating wavelength of 715 nm was chosen to optimize dye lifetime rather than photoelectron polarization. The laser produced a 600-ns pulse from which two 2-ns pulses of typically 5 μJ each (at the cathode) were optically chopped for SLC. For the 1992 fixed-target run, the dye laser pulse length was stretched to 800 ns.

For the 1993 SLC run, the dye laser was replaced with a Nd:YAG (neodymium-doped yttrium aluminum garnet) pumped Ti:sapphire laser [86], providing increased peak power and allowing operation at the wavelength required by the strained-lattice cathodes. This system was upgraded to provide better intensity stability for the 1994 SLC run (a detailed description follows in Section 8.2).

For the 1993 fixed-target run, a flashlamp-pumped Ti:sapphire laser was constructed at SLAC [87] since the YAG-pumped system could not provide the required pulse width. The required 2.2-μs pulse was chopped from an approximately 10-μs laser output pulse. This system is described in Section 8.3.

8.2. YAG-pumped Ti:sapphire laser

To meet the SLC beam requirements, the source laser was required to produce a pair of short pulses separated by 62 ns, with an overall repetition rate of 120 Hz. The first pulse was typically operated at wavelengths between 830 and 870 nm, optimized for the particular cathode in use. The second pulse produced the electrons later used to generate positrons. Note that the polarization of the second electron

bunch was not important, since the resulting positrons will in any case not be polarized. The second laser pulse was operated at ~790 nm to achieve a significantly higher QE at the cathode and thus minimize the cathode charge-limit effect on the second electron bunch. Approximately 80 μJ was required to saturate the 100-nm cathodes with the first laser pulse; see Section 9.1. A schematic of the YAG-pumped Ti:sapphire (YAG-Ti) laser system is shown in Fig.10. The system used a pair of Nd:YAG lasers each of which pumped a pair of Ti:sapphire oscillators. Pockels cells driven by fast electronics were used to control the shape and energy of the output pulses. The system was designed to operate continuously over long periods (months) with good stability and very high reliability.

Titanium-doped sapphire [88] was chosen as the active material for the laser system due to its large wavelength range (720 - 880 nm). Laser pumping of the Ti:sapphire (with frequency-doubled Nd:YAG lasers) was chosen because when the design of this laser system was started, the alternative of directly flashlamp pumping the Ti:sapphire had not been demonstrated in long term operation.

Two Nd:YAG lasers, each operating at 60 Hz, were used for pumping because there were no commercially available YAGs which met the energy requirements at 120 Hz. The Nd:YAG lasers [89] were operated with reduced lamp energy in order to provide increased flashlamp lifetime. Each of the Nd:YAG lasers produced approximately 25 mJ at 532 nm and 60 Hz, with a typical flashlamp lifetime of 4×10^8 shots (~3 months). The typical intensity jitter from the Nd:YAG lasers was 2.5% rms. The Nd:YAG lasers produced sufficient energy that the combining inefficiency (50% of the beam must be dumped) did not affect operation.

A schematic of one of the two identical Ti:sapphire cavities is shown in Fig. 11. Each cavity was Q-switched and cavity-dumped by an intracavity Pockels cell. When high voltage (1.5 kV) was applied to the Pockels cell, it rotated the optical polarization and caused any energy circulating in the optical cavity to be reflected from the intracavity polarizer. Voltage was applied to the Pockels cell before the Ti:sapphire crystal was pumped by the Nd:YAG laser. The time at which the high voltage was removed determined the

time at which oscillation began to develop. At the peak of the intracavity power, a very fast (<1 ns rise time) pulse was applied to the Pockels cell to dump the circulating power to the output. The result was a fast rise-time and fall-time pulse with a length equal to the round trip length of the optical cavity (approximately 3.5 ns).

The laser system made extensive use of feedback to maintain long-term stability. The Nd:YAG laser output energies were stabilized by a feedback that adjusted the flashlamp energy. The build-up time of the optical pulse in the Ti:sapphire cavities was controlled by a feedback which adjusts the timing for the high-voltage pulse that Q-switched the optical cavity. The output power from the Ti:sapphire cavities was also stabilized by a feedback. With these feedbacks operational, no adjustment was required during the 3 months between flashlamp changes.

The intensity stability was substantially improved by the use of a feed-forward system. The primary source of instability was fluctuation in the Nd:YAG output energy, which changed the gain and, therefore, the optical build-up time of the Ti:sapphire cavities. Since the cavity energy must be dumped at a fixed time that is set by the accelerator timing, the intracavity power when the cavity is dumped varies with Nd:YAG energy. This was corrected by a feed-forward system which measured the Nd:YAG energy on each pulse and, on the same pulse, adjusted the timing of the high-voltage Q-switch pulse to compensate for changes in gain. This system reduced the intensity noise from the laser from 5% to ~1% rms.

The output pulse from the Ti:sapphire cavity was shaped with a fast (2 ns FWHM) Pockels-cell pulse chopper used with a crossed polarizer. The intensity was controlled with a longer pulse (30 ns) Pockels cell. The beams from the two cavities were combined with a polarizing splitter. The circular polarization sign of the production bunch was controlled with another Pockels cell. The polarization sign was set randomly on each pulse to reduce systematic errors. This sign was transmitted to the data acquisition system at the experimental hall. Adjustable telescopes in the optical transport allowed independent steering and focusing of the two bunches onto the cathode.

The helicity of the laser light for a given optics installation was checked using a liquid crystal polarizer [90] for which we independently determined the sign using the method of total internal reflection [91].

8.3. Flashlamp -pumped Ti:sapphire laser

The flashlamp-pumped Ti:sapphire (flash-Ti) laser was required to produce a 2.2 μs, 80 μJ (at the cathode) pulse to meet the requirements of the fixed-target experiments. This long pulse length could not be achieved with a Q-switched system similar to the YAG-Ti laser due to the short excited state lifetime of Ti:sapphire (3.2 μs). Instead, the laser was operated in long-pulse mode where the rod was pumped continuously during the output pulse.

The flash-Ti laser used a pair of short-pulse flashlamps coupled to a Ti:sapphire rod with a dual elliptical specular reflector cavity. Ti:sapphire is difficult to flashlamp-pump due to its short excited-state lifetime and narrow absorption band (centered near 500 nm). Increases in flashlamp energy produce a hotter discharge which shifts the spectrum further into the UV with a fairly small increase in pump energy in the required band. Decreasing the pump pulse length to reduce losses due to spontaneous emission both increases the discharge temperature and decreases the flashlamp lifetime. A 7.5-μs pump pulse was chosen as a compromise between these effects.

Pure silver was used as the reflector material to optimize reflectivity. The pump chamber was flooded with high purity water for cooling and to protect the reflectors. The rod size was chosen considerably smaller than the flashlamp image in the chamber in order to maximize pumping density. The flashlamp discharge circuit used an ~6 kV thyratron modulator with a typical discharge energy of 30 J.

The output from the laser was chopped to 2.2 μs using a Pockels cell. The Pockels cell was driven by a fast high-voltage feedback amplifier that stabilized the output power during the pulse. This system reduced the laser intensity jitter from 3-4% rms to 2% rms and produced a square output pulse.

For maintenance, the laser only required flashlamp changes every $1\text{-}2\times10^8$ shots (every 10-20 days) and two coolant-filter changes during the 3-month run. The laser is being upgraded for the 1995 fixed-target run.

9. Source performance

9.1. Photoemission limitations

An important discovery in the course of polarized electron source research and development at SLAC is the so-called cathode charge-limit phenomenon introduced in Section 3.4. If the QE of an NEA GaAs cathode is below a critical value, the maximum charge that can be extracted from a cathode illuminated with a laser pulse whose wavelength is close to the band gap (a necessary energy condition for achieving high polarization) is determined by the intrinsic properties of the cathode rather than by the space charge limit. The significance of the cathode charge-limit effect lies in that it imposes a severe constraint on the usability of NEA photocathodes for polarized electron sources designed to produce high intensity beams.

Figure 12 shows the charge-versus-laser energy data along with several characteristic temporal profiles of the emitted charge pulses for a 300-nm strained GaAs(100), 14-mm cathode similar to the one used for the 1993 SLC run, excited with 865-nm laser pulses that have a 2-ns FWHM pulse width. The data show that the maximum extractable charge for this cathode, which had for this data a QE of 0.38% measured at 833 nm, was about 3.5×10^{10} electrons at 120 kV. This was more than a factor of 3 less than that allowed by the space-charge limit. In addition, once the photoemission was charge limited (or equivalently, once the cathode was saturated), a further increase in the laser pulse energy actually led to a decrease in the

photoemitted charge. The nature of the cathode charge-limit effect is best illustrated by the temporal behavior of the charge pulses shown in Fig. 12(b). For charge-limited photoemission: (i) with increasing laser pulse energy, the charge pulse peaks at an increasingly earlier time and shrinks in width as a result of suppressed emission in the later portion of the pulse, and (ii) the peak current of the charge pulse remains nearly the same, but below the space-charge limit (~9 A in this case) for varying laser energies. As the QE of the cathode decays with time, the cathode charge limit decreases proportionally while the laser energy needed to reach saturation remains constant. When the QE drops to a certain value such that the corresponding charge performance no longer meets the operating beam intensity requirement, the cathode must be recesiated as described in Section 7.3. The cathode charge-limit phenomenon can be simulated using a surface photovoltaic model [92] in which the surface barrier temporarily rises due to the large number of conduction band electrons transported to the surface that cannot be instantaneously discharged. Consequently, when comparing the charge limiting effects for different cathodes, it is the surface escape probability that is the principle indicator of peak extractable charge.

Another important aspect of the charge limit phenomenon is its memory effect on pulse trains. Figure 13 shows the maximum charge for a second 2-ns bunch as a function of time separation from the first 2-ns bunch in the 2-bunch train. It is clearly seen that for small bunch separations, the presence of a preceding bunch substantially suppresses the maximum extractable charge in the second bunch. This memory effect is found to depend critically on the doping density of the GaAs cathode material. The higher the doping density is, the faster the memory effect decays with time. On the other hand, high doping density appears to have an adverse effect on the polarization; see Section 9.6. A good compromise for SLC operation is to use cathode materials with a dopant density of about 5×10^{18} cm^{-3}. For high-energy physics programs that require polarized high-intensity long-pulse (> 10 ns) beams or long trains of microbunches (such as those proposed for the next generation of linear colliders), one may have to use more highly doped GaAs cathodes at the expense of polarization. An alternative to the uniformly high-doped strained GaAs cathode would be a strained GaAs cathode with low doping concentration ($\leq10^{18}$ cm^{-3}) in its active layer except for a high doping ($\geq10^{19}$ cm^{-3}) in the bent-band region (final ~5 nm). This technique has already

been tried with a superlattice cathode with considerable success [93], although there may be additional factors contributing to the superlattice performance.

High-energy physics experiments that use polarized electron beams almost without exception require that the spin polarization of the beam be switched, either randomly or in a prescribed way, between two opposite directions on a pulse-to-pulse basis with identical electron intensity for each polarization. With strained GaAs(100) photocathodes, we found that the QE measured with linearly polarized light at a wavelength close to the band gap threshold may vary considerably (up to ± 15%) when its polarization plane is rotated. This effect originates from partial relaxation of the strain along a preferred direction in the cathode plane, which leads to a mixing of the heavy-hole and light-hole states in the valence band. The existence of such a preferred direction is related to the existence of structural anisotropy. As circularly polarized light that is experimentally generated always contains a small component of linear polarization, it introduces an asymmetry in the photoemitted beam intensity between the two polarization states owing to the linear polarization direction effect. Thus, great care was needed to tune the two circular polarization states to minimize the beam intensity asymmetry. In practice, the charge asymmetry generated by this source could be reduced to $<5\times10^{-4}$ by adjusting the voltage on the Pockels cell used to control the sign of the circular polarization.

9.2. Source configurations

Electron sources for nonpolarized beams have developed in recent decades into highly reliable, nearly maintenance-free systems requiring only minimal manpower. The polarized electron source for the Stanford linear accelerator, although a much more complex system, has proven to have equally high reliability, and by maximizing the monitoring capabilities of the SLC computer control system, the manpower required for routine operation is also minimal.

The performance of the polarized electron source while operating for long periods under relatively steady-state conditions provides a unique window to view the factors that affect photocathode performance. The remaining sections of this report highlight the more interesting observations and the corresponding source parameters.

The four guns built for the SLC source are listed in Table 3. They are essentially identical, although the evolution of changes among the four guns was not completely in phase. The major changes since the start of polarized beam operations in April, 1992 were the addition of LoadLock in early 1993 and the doubling of the active area of the cathode that is in progress in 1994-95. With the addition of LoadLock, the Cs effusion cell in the gun was replaced with Cs channels as mentioned earlier. Beginning in 1993, all cathode activations were done in LoadLock, while all recesiations continued to be done in the gun chamber.

The process of activating a cathode takes about 8 hours. Before the advent of LoadLock, the results of each activation were highly variable. In order to insure the highest operational efficiency, it was originally anticipated that the polarized gun would have to be removed rather frequently and replaced with a gun already having a successfully activated cathode. This was the principle reason the vacuum isolation section, described earlier, was designed for rapid exchange of guns. With LoadLock, cathodes could be exchanged or re-activated with a high degree of reliability, making an exchange of guns unnecessary—although 8 to 16 hours, in addition to the activation time, was required to purge the gas-containment vessel prior to applying full bias voltage. After over 2 years of cumulative operating time, there has been no cathode or gun failure during a physics run.

The four types of cathodes that have been used are listed in Table 4. SLC operations began with VGF GaAs since the higher polarization materials were then not fully tested. In addition, only the flashlamp-pumped dye laser was available, which limited the excitation wavelength to 715 nm. Some improvement in polarization was later obtained by shifting to a thin AlGaAs cathode that had a band gap more closely matched to the laser. The real improvement in polarization came with the introduction of strained-lattice

cathodes in 1993. This was made possible by the completion of the YAG-Ti laser described in Section 8.2). The wavelength of the YAG-Ti laser could be tuned to the band gap of the strained-lattice cathodes. Initially there was uncertainty as to the maximum charge per pulse that could be extracted from the very thin cathodes because of the cathode charge limit discussed earlier. For this reason, a 300-nm strained-layer cathode was chosen in 1993. Later it was found in the laboratory that the peak charge is essentially independent of the thickness of the active layer, so that a 100-nm strained-lattice cathode with significantly higher polarization was used in 1994.

There have been five high-energy physics operating *cycles* (or *runs*) utilizing the polarized beam. The three SLC cycles in 1992, 1993, and 1994 [94] resulted in about 635 days of operation of the polarized source. Additionally, the two fixed-target experiments, E–142 and E–143, which required long pulses and relatively low peak currents, resulted in another 135 days of operation. During all of these operations, the source was operating as required for more than 95% of the time, which is comparable to the operating efficiency of the accelerator thermionic gun system. The operating parameters of the polarized source for these various periods are given in Table 5 and discussed below.

9.3. QE, lifetime, and charge

As indicated in Section 9.1 above, the cathode charge limit for a given type of cathode has been found to be proportional to the QE, up to the space charge limit of the gun. This is explained in the surface photovoltaic model as a surface effect, implying that the cathode charge limit should be proportional to the surface escape probability P independently of the cathode thickness. P can be approximated by the ratio of the measured QE to the calculated internal yield Y_{int} using Eq. 2. The values of P calculated in this manner for three of the GaAs cathodes listed in Table 4 are shown in Table 6, where the values of peak QE from Table 5 are used. Since the QE for the thin cathodes (III and IVb) was not monitored exactly at the polarization peak, an estimate of P for this condition using the measured variation of QE with λ is shown in parentheses.

The peak charge for the thick GaAs cathode (I) given in Table 5 is dominated by the space-charge limit of the gun. From Fig. 14, one can see that when the cathode charge limit for the thick GaAs cathode (excited by 715 nm light) dropped to ~6×10^{10} e^- (i.e., just before the cathode was recesiated), the QE at 750 nm was ~2.5%. Using the variation of QE with λ given in the literature [95], the QE at the band gap edge should have been about 1.3%. The value of P estimated from this QE is also shown in parentheses. The variation of the cathode charge limit with wavelength is not well characterized other than that the limit increases with decreasing wavelength, presumably due to the increase in the fraction of emitted electrons that are not fully thermalized ("hot" electrons) in the conduction band. The charge limit for the thick cathode at the bandgap is estimated to be roughly 25% lower than that measured at 715 nm based on the observed wavelength dependence of the charge limit for a 300 nm cathode [96] and also a 100 nm cathode. For all three cathodes, the ratio of the charge limit to the surface escape probability is shown in Table 6 for the band gap edge as estimated here. Given the large uncertainty in their derivation, the ratios shown are not inconsistent with the premise that they are independent of cathode thickness.

For the thin cathodes, processes other than simple diffusion may be contributing to the internal yield. Reflection of either conduction band electrons or photons at the back heterojunction could greatly increase the yield while having a correspondingly small effect on the net polarization of the emitted electrons. Readsorption of recombination light is another possible process that would increase the yield. As indicated in Ref. [27], recombination light from a very thin active layer should have a negligible effect on either the yield or the polarization. By contrast, recombination light reaching the active layer from the GaAs substrate should have very low polarization, in much the same manner as discussed in Ref. [27] for thick active layers, and may contribute significantly to the internal yield for very thin active layers.

For the SLC, the electron source was consistently operated with a charge of 6–7×10^{10} e^- in each of the two required bunches at 120 Hz. When not space-charge limited, the change in the maximum charge or QE with time is given by

$$Q(t) = Q(0)\ \exp\{-t/\tau\}\ , \qquad (4)$$

where Q can be charge or QE and τ is defined as the cathode lifetime. *Q(0)* is here always taken as the peak value following activation or recesiation.

It is well known that the cathode lifetimes are very system dependent. The lifetimes for this source while operating the accelerator are shown in Table 5 to vary from 35 hours to *infinity*. By *infinity* it is meant that the QE (without application of additional Cs) did not change during the period of operation. The source has always been operated very conservatively for the accelerator so as not to risk the high energy physics program. In some cases longer lifetimes could possibly have been achieved with additional activations or other invasive (and not risk free) procedures. In each case the total pressure in the gun chamber as well as the spectrum measured with the RGA was identical. In no case was the cathode lifetime affected by operation of the beam, although under some circumstances, as mentioned in Section 4.4, it did appear to be somewhat affected by exposure to the accelerator vacuum. The dark current, especially if more than about 100 nA, was seen to affect the lifetime. The best lifetime during SLC operations for a strained-layer cathode, 1200 hours, was achieved in a gun that had a dark current of only 10 nA [97]. Dark currents can release contaminants (including oxidizers) from the exposed surfaces in the vacuum system that can condense on the GaAs crystal, lowering the QE. It is noted that the *infinite* lifetime achieved with the AlGaAs cathode was for operation of a low peak-current beam, so that a cathode bias of only 60 kV was required. This lower bias resulted in a dark current too low to be measured. In addition, the operating QE was about an order of magnitude lower than the maximum achieved in the laboratory. Moreover, the excitation wavelength used with this cathode was quite far from the band-gap edge compared to the high-polarization operation of the strained-layer cathodes, and thus the lifetime, was presumably less sensitive to surface contamination.

Given the ease and speed with which cathodes can be recesiated, the most critical parameter for SLC is actually not the lifetime, but the peak value of the QE. Assuming the peak value of QE results in a saturated current greater than the normal operating current, the predicted maximum time between cesiations can be easily calculated from Eq. 4 using the peak and minimum operating currents or QEs.

It was our general experience that a longer lifetime was achieved when the initial QE following activation was high. Thus residual contamination on the clean surface before application of the Cs-F layer appears to either inhibit the formation of a proper Cs-F dipole on the surface, or perhaps results in a looser bonding of the excess Cs. With LoadLock, it appears always possible to achieve a high QE across the entire surface if the activation process is repeated enough times, four times being the maximum we have had to use before beginning SLC operations.

For all of the cathodes used to date, recesiating restored the QE to its initial value. A large number of activations were done in 1992 during SLC operations only because the lifetimes became so short that recesiations were required more often than once a day. In 1992, the QE following the first few recesiations steadily increased until following the second activation it was more than double its original value a—clear indication that the cathode was originally less than optimally activated. It should be noted that only in 1992 was the cathode activated after having been baked with the gun, i.e., without LoadLock.

There is an increasing accumulation of experimental evidence that no Cs is lost from the surface under normal operating conditions [98]. In a UHV stainless-steel system, the harmful residual gases that might be present include H_2O, O_2, and CO_2. In addition, at SLAC the cathode activations introduce NF_3, but only in the LoadLock chamber. After months of pumping, the residual O_2 would be expected to be significantly decreased. For contamination with CO_2, the QE should not be completely restorable by recesiating [99]. NF_3 contamination is equally unlikely, since confining the activations to the LoadLock chamber in 1993 did not significantly change the cathode lifetimes in the gun chamber. However, for contamination by water vapor, the QE should be fully restorable by adding extra Cs[99].

The cathode lifetimes, measured for individual cesiation cycles, appear to decrease with time unless excess cesium is applied when recesiating (so-called "over-cesiation"). Because of the fear of HV breakdown [100], all of the cesiations during the first half of the SLC92 run deliberately used a minimal amount of Cs. As illustrated in Fig. 14, the lifetimes progressively decreased following each cesiation for a common activation. In the second half of the run, when over-cesiation was consistently used, this pattern disappeared or at least was greatly diminished. During the SLC94 run, for which there were no re-activations after the start of the run, the cathode lifetimes remained stable at ~1200 hours during the first 3 months when all recesiations (there were 11) included over-cesiation. The liftemes then gradually dropped to ~300 hours over the next 4 months when the cathodes were only under-cesiated (17 times) to gain a few percent in the polarization; see Section 9.6. Three over-cesiations at the end of 1994 increased the house lifetimes to the level of ~600 hours. Similarly, when the 300-nm strained-layer cathode was used in 1993, there were 29 recesiations, almost all with over-cesiation, following each of the two activations during the cycle. The lifetimes remained stable at ~700 hours after the first few recesiations. It thus appears that the Cs associated with the contaminants at the time of a recesiation will migrate, perhaps combining with newly incident oxides in such a way as to lower the QE. This adds to the effect of new contaminants, and thus progressively decreases the lifetime until all the contaminants are once again removed at the next activation. It has also been suggested that the excess Cs may simply interdiffuse into the oxide layer [101], a process that may be more likely as the oxide layer gets thicker.

For all the data reported here, the cathode was operated at about 0°C. Although it was clear that there was additional surface contamination accumulated when the cathode was cooler than the rest of the gun [102], the lifetimes appeared nonetheless to be longer, perhaps because the migration or interdiffusion of excess Cs was slowed down.

Based on this experience, we speculate that there are two types of contaminants in the gun vacuum system. The first type oxidizes the excess Cs, leading to a rapid decrease in yield (Cs bonds very strongly

to oxidizers). There is no reason to think that this process should lead to a decrease in the lifetime with time as long as excess Cs is available. The second type of contaminant is presumed to bond to Cs only loosely. Consequently, as discussed above, the Cs easily migrates away.

The QE of the 300-nm cathode used in 1993 is shown in Fig. 15 for the period April through September following the second activation. No NF_3 was added during this entire period, yet the peak QE following a recesiation did not drop more than 5% overall. This data demonstrates the extraordinary stability of the Cs-F layer. It is not known if this same performance can be achieved with a Cs-O layer.

9.4. Beam stability

The beam stability is primarily a matter of laser and optical transport system stability. The intensity jitter at the cathode was progressively reduced to the point where it directly met the SLC stability requirements. Prior to 1994, it was necessary to operate the cathode partially in saturation in order to reduce the intensity jitter to <2%. This was easily achieved using a feedback loop that varied the laser spot size on the cathode until the saturated current matched the required current. Since the QE profile across the GaAs surface was not always uniform, and changed with time, changing the laser spot size tended to change the centroid of the electron beam at the cathode, making it difficult to keep the electron beam orbits in the injector constant. In 1994, with the single-mode YAG-Ti laser operating with ≤1% intensity jitter, there was no need to operate in saturation, and thus the laser spot size could be kept constant and the electron current was adjusted using a feedback loop that simply adjusted the attenuation in the laser beam. This resulted in orbits that were more stable. When combined with full cathode illumination, the single-mode laser produced an electron beam with a centroid at the gun that was stable to <10 μm rms.

Since the laser system was inaccessible for weeks at a time during accelerator operations, it was important that any drifts be detected and automatically corrected by feedback systems. The required laser feedback systems were described for the current YAG-Ti laser system; see Section 8.2.

9.5. Operational efficiency

Most of the major parameters of the laser and electron beam at the gun were monitored and history buffered by the SLC computer control program. As for all other SLC systems, parameters that fell outside their specified tolerance were called to the attention of the accelerator operations staff by a color-coded display in the main control center. The operators kept in clear view real-time video displays of the laser beam spot and of the bunched electron beam. Causes of failure in the power supplies and controls systems for the source were located, and necessary repairs were made, by the operators and supporting technical groups, as is done for other SLC systems. A physicist checked on the source performance on a daily basis. Some source parameters were adjusted infrequently through the SLC computer control program. Source physicists either performed or supervised much of the invasive maintenance, which in any case was very infrequent. Recesiations were routinely performed by the operators, who had merely to push a series of touch panel buttons.

As shown in Table 5, the operating efficiency of the source was consistently high. This was possible for such a complex system operating essentially without operator intervention, because a complete duplicate of the first 6 meters of the SLC injector (i.e., up to the injector SHB system) had been built and installed in the Gun Test Laboratory (GTL) in 1991. The lab system was monitored and controlled in exactly the same manner as in the SLC, including the same software. Although the high-power pulsed dye laser was already installed at the injector, a Laser Development Laboratory (LDL) was built in the room adjacent to the GTL to develop a tunable Ti:sapphire laser for the source to match the new strained-layer cathodes. In late 1991, the first of the four photocathode guns was successfully tested at 120 kV in the new beamline in the GTL using a 60 Hz, high-power Nd:YAG laser in the LDL. This was followed by a less than successful test at the SLC injector in which the cathode was for the first time excited by the high-power dye laser that operated significantly closer to the band-gap edge, leading to the discovery of the cathode charge limit. High-voltage breakdown at 120 kV, due in part to excessive use of the cesium

effusion cell in the gun chamber to keep the QE high, was a serious problem. Following this experience, the cathode electrode design was modified to reduce the maximum field at large radius by about 25% [103]. It was also discovered at this time that the temperature of the GaAs surface during heat cleaning was significantly lower than indicated by a thermocouple at the cathode end of the emitter tube. In addition, a NEG pump was added to the gun vacuum chamber. Further testing of guns in the GTL eventually produced a gun for the 1992 run that had a reasonably high QE after completion of HV processing. Meanwhile, the Ti:sapphire laser was completed in the LDL and thoroughly tested with the GTL system before installation at the SLC injector for the 1993 run. LoadLock was developed and tested in the same manner. The equipment and tests described here not only produced the necessary physical system, they also provided the necessary operating and maintenance experience necessary to make the source perform efficiently.

9.6. Polarization

The source polarization was determined primarily by the choice of cathode and available laser. As shown in Table 5, the polarization increased from about 25% in 1992 to over 80% in 1994 [104]. It has been known for some time that the polarization of the electrons extracted from GaAs tends to be higher if the active layer is very thin. The choice of a thick (rather than thin), unstrained [105] GaAs cathode in 1992 was driven primarily by the difficulty that was found earlier in successfully operating a thin AlGaAs cathode activated and processed at high voltage without LoadLock. A long lifetime with an AlGaAs cathode despite having no LoadLock was later achieved for E–142, in part because the required operating voltage was only 60 kV.

The residual strain created in a thin layer of GaAs by a lattice mismatch introduced at the heterojunction with the sublayer decreases as the thickness of the active layer is increased. Both the minimum band-gap energy and the maximum electron polarization decrease with decreasing residual strain [9], [28], so that with increasing thickness of the active layer, the peak polarization should decrease and the

excitation wavelength corresponding to the polarization peak should increase, approaching the band gap for unstrained cathodes. This effect is confirmed by the operating wavelengths required to produce the peak polarizations for the 100- and 300-nm strained-layer cathodes (III and IV) as shown in Table 5.

Before a GaAs cathode material was used for SLC operation, its peak polarization and maximum charge produced with a 2-ns laser pulse of wavelength close to its band gap threshold was measured and shown to meet the SLC requirements. At SLAC, polarization measurements could be performed at low energy in three separate systems, one of which was also capable of characterizing a cathode's charge performance. Starting in 1994, a 108° electrostatic bend that rotates the polarization vector of a 100 keV electron beam from longitudinal to transverse orientation [106] and a Mott polarimeter were added to the beamline in the GTL. Coupled with a YAG-pumped Ti:sapphire laser system that duplicated the system at the SLC injector, this test facility is capable of characterizing both the polarization and charge performance of a cathode. A load-locked Cathode Test System (CTS) that uses two sets of electrostatic cylindrical lens triplets for beam transport, a 90° electrostatic bend for yielding transverse polarization, and a medium energy (20–30 keV) retarding-field Mott polarimeter that was commissioned at SLAC in 1993 is ideal for quick polarization measurements at low electron energies (tens of eV). A plot of the electron beam polarization P_e and the corresponding QE as a function of wavelength measured with this polarimeter for a 100-nm strained-lattice crystal from the same wafer as IV in Table 4 is shown in Fig. 6. A third system (PEGGY) that uses a first generation SLAC polarized electron gun [4], a set of beam transport magnetic optics, a Wien filter for spin manipulation at 60 keV, and a Mott polarimeter has been in use for polarization studies at SLAC since the mid 1980s [107].

For the SLC, the longitudinally polarized electrons generated by the source are first accelerated to ~1.2 GeV, the damping ring energy. Before entering the damping ring, the spin vector is rotated vertical with the first spin rotation solenoid shown in Fig. 1(a). There is a 1% (5% in 1992) relative depolarization in the damping ring since it is not operated at the exact design energy. After extraction from the damping ring, the beam is accelerated to ~50 GeV with the spin vector still vertical. In the Collider Arc, spin bumps

are used to align the spin vector longitudinal at the interaction point [108]. The Arc introduces a relative depolarization of 1–5% depending on the configuration [109]. The longitudinal component of the electron polarization is measured just after the interaction point using a Compton polarimeter. Two additional spin rotators that are located after the damping ring allowed acceleration of electrons with any desired spin orientation in the linac for diagnostic purposes. The polarization at the end of the linac and before the Collider Arc could be measured using the Linac Møller polarimeter.

For fixed-target experiments, the longitudinally polarized beam was accelerated without damping directly to the End Station A as shown in Fig. 1(b). There is no significant depolarization mechanism in this accelerating system. The electron polarization is measured using the ESA Møller polarimeter located just before the target.

During operation of this source, the polarization was observed to increase with decreasing QE [110]. This effect appears to be related to a reduction in the emission probability of thermalized relative to "hot" electrons because of the increase in the surface barrier. Hot electrons have a very short escape depth, thus they presumably have undergone less depolarization. For the SLC runs with the relatively thin, strained GaAs cathodes, the QE had to be maintained near its maximum value (i.e., approximately constant) to produce the desired electron intensity of several amperes. Thus there was only a small variation in polarization associated with the QE. However, in the 1993 fixed-target experiment, E–143, for which the 100-nm strained GaAs cathode was first introduced, a very low intensity (<1 mA peak current at the source) 2-μs pulse was required. Thus the QE was allowed to drop very low--more than a factor of 10 below the peak value that could be achieved following a full recesiation. Under these conditions the polarization was found to increase significantly, averaging 86% [111], [112] at the lowest QEs compared to ~75% at the highest QE. The polarization at the source is shown in Fig. 17 as a function of QE measured by two different polarimeters. The photocathodes associated with each polarimeter measurement were from a similar portion of the same 100-nm strained-lattice GaAs wafer (SPIRE MO5-2667).

From Fig. 17, it appears that even at zero yield, the polarization will not be 100%. In practice, the theoretical maximum polarizations are never realized. For strained cathodes, insufficient splitting of the heavy-hole and light-hole bands would limit the polarization, since the rms variation in the band tailing at room temperature is expected to be on the order of 30 meV for the doping concentrations in the range of 5×10^{18} cm^{-3} [30]. The calculated band splitting for the 100-nm cathodes (cathodes IV and V in Table 4) is on the order of 50–60 meV, which should be sufficient, but strain relaxation is expected to begin when the thickness of the active layer exceeds a critical thickness calculated to be on the order of 10 nm [9], [28]. Once an electron is promoted to the conduction band, it is very difficult to flip its spin unless the electron kinetic energy is greater than the band gap. Several mechanisms for spin flip have been proposed [113], but to date there is no convincing experimental clarification for room temperature cathodes with medium to high doping concentrations. Radiation trapping [27] is one possibility that is consistent with the observed variation of the photoemitted electron polarization with both temperature and thickness of the semiconductor active material. Finally, it appears that P_e may decrease slightly as the doping concentration increases above 10^{18} cm^{-3} [114].

There are no known surface depolarization effects, although spin-exchange electron scattering from free Cs could conceivably reduce the polarization [115].

10. Summary

A high peak intensity polarized electron source based on photoemission from various semiconductor photocathodes has been developed at SLAC. Valence band electrons are photoexcited into the conduction band of the photocathode using circularly polarized light from SLAC-built pulsed, tunable lasers operating at the band-gap energy. Polarized electrons are extracted at high voltage by treating the surface of the semiconductor to be NEA. The source has now been operated nearly continuously for 3 years, with insignificant downtime, to provide all the electron beams for the SLAC 3-km accelerator. High peak current (several amperes) short bunches (2 ns) have been generated at the source for SLC. Longer bunches

(several microseconds) with lower peak intensities (up to 20 mA) have been produced at the source for the fixed targets.

Important features incorporated into this source include a system to rapidly and reliably install and remove photocathode crystals into and from the gun without breaking the vacuum of the gun chamber itself, permitting the gun to be processed for high voltage before installing a cathode. The cathodes are activated outside the gun chamber. After installation of the cathode in the gun, application of cesium to the cathode surface takes only a few minutes using a computer controlled process initiated by the accelerator operators. The yield of photoelectrons is high enough and the rate of decrease of the yield is slow enough to permit several days of accelerator operations between recesiations. No other adjustments to the source are needed until the laser flashlamps are changed after several months of operation. The source is extensively monitored and the results recorded every 6 minutes by the accelerator computer control system.

The decrease of the quantum efficiency was unaffected by the operation of the electron beam. It was also only very weakly affected, if at all, by the high voltage if the dark current was kept below ~50 nA.

The polarization of the electron beam has been increased to the level of 80% by using thin, strained-lattice cathodes. The maximum charge that can be extracted in a given pulse from GaAs photocathodes has been shown to be controlled by the surface conditions. In general, the maximum charge increases as the low-intensity quantum yield increases until the space charge limit of the gun is reached. On the other hand, this cathode charge limit has been shown not to decrease significantly as the thickness of the active layer of thin cathodes is decreased, making possible the application of strained-lattice cathodes for the SLC.

The success of the polarized electron source has enabled the Stanford linear accelerator to accommodate a very competitive high-energy physics program. Largely because of this success, the SLC is scheduled to continue operating through 1998, and at least two new fixed-target experiments, E–154 and E–155, have been scheduled for 1995 and 1996, respectively.

Future colliders will also operate with polarized electrons. The Stanford source described here provides a well-characterized base model which will be important for the design of the next generation polarized electron source.

Acknowledgments

A large part of the SLAC technical staff has contributed to the success of the polarized electron source described here. We here acknowledge their cooperation and professional skills with sincere thanks and appreciation. Certain individuals have made significant contributions. These include M. Browne, G. Collet, K. Eppley, E. Garwin, K. Harris, W. Herrmannsfeldt, T. Lavine, T. Maruyama, T. Montagne, A. Odian, R. Prepost, K. Ratcliffe and D. Wright. In addition, we recognize the early contributions by S. Kaiser, K. Moffeit, F. Perrier and D. Walz. The efforts of C. Sinclair in the early development of a polarized electron source for the SLC and his continuing interest and advice have been particularly valuable.

References

[1] Reviews of the production and uses of polarized electrons can be found in R. Feder, *Polarized Electrons in Surface Physics* (Singapore: World Scientific, 1985) 610 pp.; J. Kessler, *Polarized Electrons*, 2nd ed. (Berlin: Springer-Verlag, 1985) 299 pp.; J. Kirschner, *Polarized Electrons at Surfaces* (Berlin: Springer-Verlag, 1985) 158 pp; and B.W. Montague, Physics Reports 113 (1984) 1. Reports on recent advances in polarized electron sources can be found in the proceedings and summaries of the Workshop on Polarized Electron Sources and Polarimeters conducted in 1988, 1990, and 1992, as part of the International Symposia on High Energy Spin Physics: K.J. Heller, ed., *High Energy Spin Physics*, AIP Conf. Proceedings No. 187 (New York: Amer. Inst. Phys., 1989) 1605 pp. in 2 vols.; *High Energy Spin Physics,* vols. 1 and 2 (Berlin: Springer-Verlag, 1991) K.-H. Althoff and W. Meyer, eds., vol. 1, 651 pp., and W. Meyer, E. Steffens, and W. Thiel, eds., vol. 2, 393 pp.; and T. Hasegawa et al., eds., *Frontiers of High Energy Spin Physics* (Tokyo: Universal Academy Press, 1993) 950 pp. Additional advances in cathode material for polarized sources are reported in M. Chatwell et al., eds., *Proc. of the Workshop on Photocathodes for Polarized Electron Sources for Accelerators*, SLAC Report 432 Rev. (1994) 466 pp.

[2] M.J. Alguard et al., Nucl. Instrum. and Meth. 163 (1979) 29.

[3] E.L. Garwin et al., Helv. Phys. Acta 47 (1974) 393.

[4] C.K. Sinclair et al., in M.L. Marshak, ed., *High Energy Physics with Polarized Beams and Polarized Targets*, AIP Conf. Proceedings No. 35 (New York: Amer. Inst. Phys., 1976) p. 424.

[5] For a 6-week high-energy physics experiment, the source successfully produced a 1.6-μs pulse at 180 pps with a peak current of 15 mA using a bulk GaAs cathode operated at about 100 K and a dye laser operating at 715 nm.

[6] P. Zorabedian, Ph.D. thesis, Stanford University, SLAC Report 248 (1982) 111 pp; practical considerations precluded development of a source using this technique.

[7] T. Maruyama et al., Phys. Rev. Lett. 66 (1991) 2376.

[8] T. Nakanishi et al., Phys. Lett. A 158 (1991) 345.

[9] T. Maruyama et al., Phys. Rev. B 46 (1992) 4261.

[10] *SLC Design Handbook* (December 1984).

[11] J.T. Seeman, Ann. Rev. Nucl. Part. Sci. 41 (1991) 389.

[12] The response time of photoemission from bulk GaAs at the picosecond level is not yet fully known. See C.C. Phillips et al., J. Phys. D: Appl. Phys. 17 (1984) 1713. Recently an upper limit of about 30 ps for the photoemission response time of GaAs has been measured for certain experimental conditions. See P.V. Logatchev et al., "Measurement of Time Response of Laser-Triggered GaAs Photocathode," contributed to the *1994 European Particle Accelerator Conference,* May 17–23, 1994, London, UK.

[13] M.B. James and R.H. Miller, IEEE Trans. on Nucl. Sci. NS-28 (1981) 3461.

[14] J.E. Clendenin et al., *Proc. of the 1984 Linear Accelerator Conference,* Seeheim, FRG, p. 457.

[15] However, for machine physics studies, $\geq 10^{11} e^-$ per bunch was sometimes required from the source.

[16] R.L. Bell, *Negative Electron Affinity Devices* (Oxford: Clarendon Press, 1973) 148 pp.

[17] There is a large literature of studies of Cs plus O_2 activation of semiconductor surfaces, but almost none for Cs plus NF_3. Hence the discussion in this section is primarily for O_2 as the oxide.

[18] G. Vergara et al., Surf. Sci. 278 (1992) 131.

[19] M. Miyao et al., Appl. Surf. Sci. 33/34 (1988) 364.

[20] Note that CsF is the only known combination of F with Cs.

[21] W.E. Spicer, Phys. Rev. 112 (1958) 114.

[22] I. Kudman and T. Seidel, J. Appl. Phys. 33 (1962) 771.

[23] Strictly speaking, for thin cathodes this expression is valid only for a special value of the recombination velocity at the back heterojunction for conduction band electrons. The more general expression is given by Eq. 6.8 in Ref. [16].

[24] K. Beyzavi et. al., Appl. Phys. Lett 58 (1991) 1268

[25] J.S. Escher, "NEA Semiconductor Photoemitters," in R.K. Willardson and A.C. Beer, eds., *Semiconductors and Semimetals*, vol. 15 (New York: Academic Press, 1981) p. 248, Table IV.

[26] C.K. Sinclair, in K.J. Heller, ed., *High Energy Spin Physics*, AIP Conf. Proc. No. 187 (New York: Amer. Inst. Phys., 1988) p. 1412.

[27] A partial compilation of published polarization results for GaAs by cathode thickness and temperature, as well as other relevant parameters such as dopant concentration, is given in M. Zolotorev et al., *Proc. of the Workshop on Photocathodes for Polarized Electron Sources for Accelerators*, SLAC Report 432 Rev (1994) p. 436.

[28] H. Aoyagi et al., Phys. Lett. A 167 (1992) 415.

[29] With the degeneracy removed, the distinction between heavy and light holes disappears, but the symmetries at zero momentum remain.

[30] H.C. Casey, Jr. and F. Stern, J. Appl. Phys. 47 (1976) 631.

[31] H. Tang et al., "Experimental Studies of the Charge Limit Phenomenon in NEA GaAs Photocathodes," SLAC–Pub–6515 (1994) contributed to the *1994 European Particle Accelerator Conference,* May 17–23, 1994, London, UK; and M. Woods et al., J. Appl. Phys. 73 (1993) 8531. See also C.A. Sanford and N.C. MacDonald, J. Vac. Sci. Technol. B 8 (1990) 1853.

[32] An alternate design, in which the HV electrode is supported inside a metal vacuum chamber by several small diameter insulator tubes is described in M. Breidenbach et al., Nucl. Instrum. and Meth. A 350 (1994) 1.

[33] R. Koontz et al., IEEE Trans. Nucl. Sci. NS-28 (1981) 2213.

[34] In fact, the thermionic gun was used to commission not only the SLC injector, but also the entire SLC system, exclusive of polarization.

[35] C.K. Sinclair and R.H. Miller, IEEE Trans. Nucl. Sci. NS–28 (1981) 2649.

[36] EGUN is a computer code for electron optics and gun design. See W. Herrmannsfeldt, SLAC Report 331 (1988) 129 pp.

[37]For illumination of the cathode with a round spot of radius r having transverse intensity distributions that are square, the maximum current varies as $r^{3/2}$. The temporal intensity distribution is assumed here to be flat within the 2-ns window accepted by the injector bunching system.

[38] The crystal itself has a 22.5-mm diameter. Before 1994, the cathode hole diameter was 14 mm (crystal 18 mm).

[39] The ceramic is type AD300 or AD94 alumina, manufactured by Coors Ceramic Co., Golden, CO 80401, to SLAC specification No. PS–202–100–02–R0 (1989). The specifications for the ceramic material, as well as the welding eyelets, follow the design of the SLAC 5045 klystron. The length of the ceramic was chosen to allow substitution of 2 flanged SLAC 5045 klystron ceramic insulators if necessary.

[40] This is the same material that was used for the cathode electrodes of the SLAC 5045 klystrons.

[41] P. Sáez et al., *Proc. of the 1993 Particle Accelerator Conference*, Washington, DC, p. 3033.

[42] With the pumps mounted above the cathode area as shown, macroscopic particles can fall down on the electrodes, potentially creating a dark current source .

[43] The NEG pump is also processed before the gun bakeout.

[44] Without the NEG pump, the partial pressure of H_2 was nearly an order of magnitude higher.

[45] The only verification of the accuracy of the factory calibration of the RGA was to compare the RGA and ion pump readings at a high pressure of N_2.

[46] T.L. Lavine et al., *Conf. Record of the 1991 IEEE Particle Accelerator Conference*, San Francisco, CA, p. 2284.

[47] The isolation section is baked at about 200°C using heater tapes. Although the gun isolation valve gets hot during this process, the pressure rise in the gun is minimal and there seems to be no lasting effect on the gun vacuum. In fact, a test done with an activated cathode in the gun during a bake of the isolation section showed no deterioration of the QE due to the bake.

[48] K.R. Eppley et al., *Conf. Record of the 1991 IEEE Particle Accelerator Conference*, San Francisco, CA, p. 1964.

[49] A.D. Yeremian et al., *1992 Linear Accelerator Conference Proceedings*, Ottawa, Canada, p. 353

[50] R.V. Latham, *High Voltage Vacuum Insulation: The Physical Basis* (London: Academic Press, 1981) p. 51ff.

[51] R.V. Latham and N.S. Xu, Vacuum 42 (1991) 1173.

[52] It has been shown that baking a vacuum system that has already been processed can re-activate some emission sites. See, for example, S. Bajic and R.V. Latham, J. Phys. D: Appl. Phys. 21 (1988) 943.

[53] Note that HV discharges can also occur during normal operation of the source, especially if the initial HV processing has been left incomplete in order to preserve the cathode.

[54] Polaroid TPX System, Polaroid Corp., Cambridge, MA 02139.

[55] Pure xenon has also been used.

[56] The problem of contamination of the cathode during bakeout was recognized by at least the early 1970s. See L.W. James et al., J. Appl. Phys. 42 (1971) 4976; also B.J. Stocker, Surf. Sci. 47 (1975) 501.

[57] That a high initial QE can more readily be attained in a reliable manner by not baking the cathode with the gun was first pointed out to us by J. Edgecumbe in 1990. Subsequently, we experimentally confirmed this observation for bulk GaAs using the low voltage cathode testing system described in C.L. Garden et al., *Proc. of the 1993 Particle Accelerator Conference,* Washington, DC, p. 3039.

[58] R.E. Kirby et al., *Proc. of the 1993 Particle Accelerator Conference,* Washington, D.C., p. 3030.

[59] R.W. Berstein and J.K. Grepstad, J. Appl. Phys. 68 (1990) 4811, and J. Vac. Sci. Technol. A7 (1989) 581.

[60] P. Brown, New Scientist (Feb. 16, 1991) p. 16; also see Material Safety Data Sheet 081, Matheson Gas Products, Secaucus, NJ 07096.

[61] The gradient freeze technique is described in V. Swaminathan and A.T. Macrander, *Materials Aspects of GaAs and InP Based Structures* (Englewood Cliffs: Prentice Hall, 1991) p. 47 ff.

[62] Manufactured by American Xtal Technology, 6780 Sierra Court, Suite 1, Dublin, CA 94568.
[63] T. Maruyama et al., J. Appl. Phys. 73 (1993) 5189.
[64] Manufactured by Spire Corp., One Patriots Park, Bedford, MA 01730.
[65] The uniformity of the strain in the larger 7.5-cm wafers is not well established.
[66] B. Schwartz, F. Ermanis, and M. H. Brastad, J. Electrochem. Society: Solid State Sci. and Tech. 123 (1976) 1089. Typically, an anodization potential of 5 V is used which yields a 100-Å-thick cap.
[67] Kodak projector cover slides catalog number 1402130.
[68] All solvents meet or exceed the Semiconductor Equipment and Materials Institute standards.
[69] The etch consisted of immersion in 30% NH_4OH at room temperature for 20 seconds.
[70] VGF GaAs was etched for 10 s in the 4:1:1 solution with the temperature of the etchant >30°C, but < 80°C.
[71] The oxide layer has been found to cause a delamination between the braze material (NiCoro 80) and the Kovar surface.
[72] MODLINE V series radiation thermometer, IRCON, Inc., Niles, IL 60648.
[73] J.S. Blakemore, J. Appl. Phys. 53 (1982) R123.
[74] The cooling rate is increased by flowing room temperature N_2 gas through the bottom of the emitter tube.
[75] W. Klein, Rev. Sci. Instrum. 42 (1971) 1082. An effusion cell was initially chosen for activating cathodes primarily for fear of running out of Cs during a long SLC run. As it happens, activations while running are rarely needed. Consequently, it is planned to replace the effusion cell used for activating with channel cesiators.
[76] Over Systems, 2553 Folsom St., San Francisco, CA 94110.
[77] G–10 is a glass cloth-epoxy resin composite. See ASTM specification D709–78.
[78] Prior to the introduction of LoadLock in 1993, when cathodes were activated in the gun chamber, a Cs effusion cell was used in the gun chamber. See Ref. [75].
[79] The dispenser channels are wired as two independent circuits. Each circuit has two dispensers in series.
[80] Additional NF_3 was not added during recesiations.
[81] F.C. Tang et al., Rev. Sci. Instrum. 57 (1986) 3004.
[82] Tubulation consisted of a 3/8-inch OD Teflon tube with bulkhead fitting (Swagelok SS–6BHT–48 without braid) surrounded by a 5/8-inch and additionally a 7/8-inch Teflon tube. The three tubes were separated by 1/16-inch PTFE wrapped as a mesh.
[83] D. Schultz et al., *Proc. of the 10th International Symposium on High Energy Spin Physics*, Nagoya, Japan (Tokyo: Universal Academy Press, 1993) p. 833.
[84]In 1992 and earlier, when a cathode was heat cleaned in the gun following about a week of operation, approximately 4 and 1 μLangmuirs (1 Langmuir = 10^{-6} Torr-sec) of CO and CO_2 respectively were released at about 100°C if the cathode had been operated at 0°C. No similar gas burst was apparent if the cathode was operated at room temperature.
[85] M. Woods et al., *Proc. of the 10th International Symposium on High Energy Spin Physics*, Nagoya, Japan (Tokyo: Universal Academy Press, 1993) p. 865.
[86] J. Frisch et al., *Proc. of the 1993 Particle Accelerator Conference,* Washington, DC, p. 3047.
[87] K.H. Witte, *Proc. of the International Conference on Lasers '93*, Lake Tahoe, CA (McLean, VA: STS Press, 1994) p. 638.
[88] A. Sanchez et al., IEEE J. Quantum Electron. 24 (1988) 995.
[89] Continuum Model NY60–60 slightly modified by SLAC.
[90] Meadowlark Optics, 7460 Weld County Road 1, Longmont, CO 80504–9470.
[91] M. Woods, "Generation of Positive or Negative Helicity Laser Light by the Fresnel/Zolotorev Method," SLD Note 223 (1992) unpublished internal report.
[92] A. Herrera-Gómez and W.E. Spicer, Proc. SPIE 2022 (1993) 51.
[93]Y. Kurihara et al., Jpn. J. Appl. Phys. 34 (1995) 355.
[94] The SLC94 run is scheduled to last until March 1995. However, only data from calendar year 1994 is included in this paper.
[95] J.S. Escher, op. cit., p. 215, Fig. 12.
[96] H. Tang et al., *Proc. of the 1993 Particle Accelerator Conference,* Washington, DC, p. 3036.
[97] Another factor that may be important in explaining this long lifetime was that although the GaAs crystal was new, the gun chamber itself had been under vacuum continuously for more than a year. See also R. Calabrese et al., Rev. Sci. Instrum. 65 (1994) 343.
[98] H. Fischer et al., *Proc. of the Workshop on Photocathodes for Polarized Electron Sources for Accelerators*, SLAC Report 432 Rev. (1994) p. 249; also R. Calabrese et al., Appl. Phys. Lett. 65 (1994) 301.
[99] T. Wada et al., Jpn. J. Appl. Phys. 29 (1990) 2087.
[100] The earlier HV breakdown experience, described in Section 9.5, was associated with the difficulty of controlling

the amount of Cs applied when using an effusion cell. Channel cesiators, for which control of the amount of applied Cs is much better, were installed in the guns in early 1993, after which the effusion cells in the guns were no longer used.

[101] M. Miyao et al., Appl. Surf. Sci. 33/34 (1988) 364.

[102] The evidence is from experience in the laboratory comparing outgassing rates for certain gas species when the cathode was heated (as part of a re-activation) following operation with the cathode at various temperatures.

[103] The low field electrode design was first suggested by W. Herrmannsfeldt (SLAC).

[104] The values of electron polarization in Table 5 are consistent with Compton polarimeter measurements corrected for known depolarizations in the electron Damping Ring and Collider Arc.

[105] In early 1992, practical strained-layer cathodes were still in the development stage.

[106] The electrostatic bend is a copy of the design described in D.A. Engwall et al., Nucl. Instrum. and Meth. A324 1993) 409.

[107] T. Maruyama et al., Appl. Phys. Lett. 55 (1989) 1686.

[108] T. Limberg et al., *Proc. of the 1993 Particle Accelerator Conference,* Washington, DC, p. 429.

[109] P. Emma et al., "Depolarization in the SLC Collider Arcs," SLAC–PUB–6527 (1994) presented at the *1994 European Particle Accelerator Conference,* May 17–23, 1994, London, UK

[110] D. Schultz et al., "The Polarized Electron Source of the Stanford Linear Accelerator Center," SLAC-PUB-6606 (1994) presented at the *17th International Linear Accelerator Conference*, Aug. 21–26, 1994, Tsukuba, Japan.

[111] K. Abe et al., Phys. Rev. Lett. 74 (1995) 346.

[112] For this very low QE, the cathode charge limit became severe even for the low electron intensities required, causing a droop in the temporal profile of the 2-μs pulse.

[113] Summarized in S.F. Alvarado et al., Z. Phys. B-Condensed Matter 44 (1981) 259; also see G. Fishman and G. Lampel, Phys. Rev. B 16 (1977) 820.

[114] Y. Kurihara et al., Nucl. Instrum. and Meth. A313 (1992) 393.

[115] M. Erbudak and B. Reihl, Appl. Phys. Lett. 33 (1978) 584.

[116] M.J. Fero representing the SLD Collaboration, in L. Vassilian, ed., *Proc. of the Twentieth Summer Institute on Particle Physics, S*LAC Report 412 (1993) p. 341.

[117] P.L. Anthony et al., Phys. Rev. Lett. 71 (1993) 959.

[118] K. Abe et al., Phys. Rev. Lett. 73 (1994) 25.

[119] T. Kaneto et al., Appl. Phys. Lett. 63 (1993) 48.

[120] P. Steiner et al., "E143 Double Arm Polarimetry—A Summary," SLAC–PUB–6728 (1995), forthcoming.

Table 1. SLC electron source beam requirements

Accelerating rf	2.856 GHz
rf pulse repetition rate	120 Hz
Bunches per rf pulse	2
Nominal bunch separation	61.625 ns
Bunch length	2.0 ns FWHM
Intensity	10^{11} e^- per bunch
Charge outside 3 ns window	$<10^9$ e^-
Intensity jitter	<1.0% rms
Position jitter	<50 μm rms
Position drift	<100 μm
Timing jitter	<50 ps rms
Invariant emittance	10^{-5} m-rad rms
Kinetic energy	120 keV
Energy jitter	$<5\times10^{-2}$% rms
Source efficiency	>95%

Table 2. Typical gun RGA data

Mass Number	Species	Partial Pressure (Torr)
2	H_2	1×10^{-11}
4	He	5×10^{-14}
12	C	3×10^{-13}
14	N	1×10^{-13}
16	CH_4, O	5×10^{-13}
18	H_2O	2×10^{-13}
28	CO, N_2	2×10^{-12}
32	O_2	2×10^{-14}
44	CO_2	$<1\times10^{-14}$

Table 3. Photocathode Guns

Gun 1. Configured with a Cs effusion cell and a 14-mm diameter cathode for E–142. Gun reconfigured for E–143 and pre-SLC94 with LoadLock, Cs channels, and a 20-mm cathode.

Gun 2. Configured with LoadLock, Cs channels, and a 14-mm diameter cathode. Used for SLC93 and SLC94.

Gun 3. Configured with a Cs effusion cell and a 14-mm diameter cathode for SLC92.

Gun 4. Configured with LoadLock, Cs channels, and 20-mm cathode.

Table 4. Cathodes

Cathode I. VGF-grown GaAs(100), Zn doped to 2×10^{19} cm^{-3} (AXT 740177).

Cathode II. MBE-grown, 300-nm $Al_{0.12}Ga_{0.88}As$(100), Be doped to 6×10^{18} cm^{-3} (U.C. Berkeley).

Cathode III. MOCVD-grown, 300-nm strained-layer GaAs(100), Zn doped to 5×10^{18} cm^{-3}, on $GaAs_{0.74}P_{0.26}$ sublayer (SPIRE MO5–1684).

Cathode IV. MOCVD-grown, 100-nm strained-layer GaAs(100), Zn doped to 4×10^{18} cm^{-3}, on $GaAs_{0.69}P_{0.31}$ sublayer (SPIRE MO 5–667). Crystal IVa has a 22.5-mm diameter while crystal IVb, cut from a similar area of the same wafer, has an 18-mm diameter.

Cathode V. MOCVD-grown, 100-nm strained-layer GaAs(100), Zn doped to 4×10^{18} cm^{-3}, on $GaAs_{0.69}P_{0.31}$ sublayer (SPIRE MO5–2768).

Note: The abbreviations for the growth techniques are defined in Section 7.1.

Table 5. Source operating parameters

	SLC92	E–142	SLC93	E–143	Pre-SLC94	SLC94
1. Source efficiency						
Operating time (hour)	3980	1062	5264	2160	~1175	4824
Availability of source (%)	~93	96	>97	>95	>95	~99
Number of activations	6	1	2	1	2	1
Recesiations per activation	6	0	29	32	26	31
Lamp/dye changes	17	5	6	7	0	2
2. Gun parameters						
Gun number	3	1	2	1	1	2
Cathode: Type	I	II	III	IVa	V	IVb
Temperature (°C)	0	0	0	0	0	0
Bias (kV)	–120	–60	–120	–60	–120	–120
Dark current (nA)	?	~0	<50	<50	50 → 250	10
QE: Peak (%)	6–10	0.8	1	0.2	0.3	0.26
Operating(%)	>4	0.8	>0.9	0.007–0.08	>0.18	>0.16
At λ (nm)	750	750	833	833	833	833
1/e lifetime (hour)	200	∞	700	35	60	1200–300
3. Laser system parameters (evaluated at cathode)						
Laser type	Dye	Dye	YAG-Ti	Flash-Ti	YAG-Ti	YAG-Ti
Operating λ (nm)	715	715	865	845	845	845
Maximum energy (μJ)	10 → 2	8	80	~75	120	120
rms intensity jitter (%)	~4(a)	~2(b)	~3	~2(c)	1.5	~1%
rms timing jitter (ps)	<50		<50		<50	<50
4. Electron beam extracted from source						
e^- pulse width (ns FWHM)	2.5	800	2.0	2200	2.0	2.0
10^{10} e^-/bunch: peak	SCL(d)	NA	7	NA	12	9
operating	6	<20	6	<0.3	6	7
rms intensity jitter (%)	≤2.5	~2	~1	~2	<1	<1
rms position/radius (%)			<7		<5	<5
Polarization at source(e) (%)	25[116]		35(f)	65	83-86[111],[120]	~80

(a) Laser jitter, ~3%, was amplified at limiting aperture in optical transport system due to multimode structure.
(b) The laser jitter listed here is after a reduction by a factor of ~2 by the electro-optical pulse chopping system.
(c) Although the laser itself was sometimes this stable, an electro-optical pulse shaping system guaranteed this performance at all times.
(d) At 120 kV, the space charge limit (SCL) is ~11×10^{10} e^- in a 2.0-ns pulse for the 14-mm diameter cathode, and is ~19×10^{10} e^- for the 20-mm cathode.
(e) Measured with the CTS Mott when not otherwise indicated.
(f) Consistent with ESA MØller[117] and PEGGY Mott [63] measurements when the original measurements are corrected using the 1993 Compton results[118].

Table 6. Surface escape probability *P* for GaAs

Cathode[a]	I	III	IVb
Thickness (nm)	thick 300	100	
λ (nm)	750 (865)	833 (865)	833 (845)
α (μm^{-1})	1.5 (0.5)	1.0 (0.5)	0.7 (0.5)
ζ	1.0	0.85[b] (0.75)	0.75
D ($cm^2 s^{-1}$)	40[119]	25[24]	25[24]
τ_e (ns)	0.75[c]	3[24]	3[24]
L (μm)	1.7	2.7	2.7
Y_{int} (%)	50 (32)	11 (7)	3.5 (2.5)
QE_{peak} (%) @120 kV	10 (1.3)	1.0 (0.25)	0.26 (0.13)
$P(\%) = \frac{QE_{peak}}{Y_{int}}$	20 (4)	9 (3.5)	7 (5)
$\frac{\text{Charge Limit}(10^{10} e^-)}{P(\%)}$	(1.1)	(2.0)	(1.8)

(a) See Table 4.

(b) The value of ζ is estimated for excitation 32 nm from the polarization peak.

(c) The lifetime shown here is scaled inversely with doping concentration from the value in reference [24].

Figure captions

1. The Stanford linear accelerator configured for: (a) SLC, and (b) fixed-target experiments. The precession of the spin vector relative to the momentum is represented in the figure by cork screws.
2. The SLC injector beamline up to 40 MeV.
3. Energy level diagram and transition probabilities at Γ point. Only the transitions for σ- excitation are shown. (a) For GaAs, the solid-line transitions are for $E_g<h\nu<(E_g+\Delta)$. (b) For GaAs-$GaAs_{1-x}P_x$, the solid-line transitions are for $E_g<h\nu<(E_g+\delta)$.
4. Longitudinal cross section of the gun.
5. Equipotential lines (dotted) in equal steps and electron trajectories calculated by EGUN for a cathode bias of -120 kV. Only the upper half of the cathode-anode cross section is shown. The 10-mm radius of the photocathode is fully illuminated. The electron beam, exiting to the right, has a waist near the anode when the cathode emission is space charge limited as shown.
6. Transverse cross section of gun vacuum chamber. The magnetic shielding for the RGA is not shown. Dimensions are approximately to scale.
7. Cutaway of LoadLock mechanics showing the linear motions, valve positions, fork assembly, emitter tube, and cathode puck.
8. (a) Cross section of cathode puck assembly and the mating portion of the cathode electrode. The Mo puck seats on the stainless steel electrode. The alumina is a docking guide. When seated there is a ~0.1 mm clearance between crystal and surrounding materials. (b) Photograph of a cathode puck with crystal attached.
9. The layer structure of the strained GaAs photocathode (cathode IV in Table 4). All layers are grown by MOCVD and p-doped with Zn to a density of 4×10^{18} cm^{-3}.
10. YAG-Ti laser system.
11. Ti:sapphire cavity for the YAG-Ti laser system.
12. Response of a 300-nm 5×10^{18} cm^{-3} Zn-doped strained GaAs(100) cathode having a QE at 833 nm of 0.38%: (a) variation in photoemitted charge as laser pulse energy is attenuated; and (b) representative charge pulse shapes at several laser pulse energies. The wave form "A" is identical to the laser pulse shape.
13. Normalized maximum charge in second bunch versus time separation from first bunch for (a) a 5×10^{18} cm^{-3} and (b) a 2×10^{19} cm^{-3} Zn-doped 300-nm strained GaAs(100) cathode with the first bunch just into the cathode charge limit (o) and deep into the charge limit (Δ). The laser wavelengths for the two bunches are 775 nm and 865 nm respectively.
14. Quantum efficiency (750 nm and 120 kV) for first two activation cycles at the SLC injector for the 1992 SLC run. "A" indicates activation (heat cleaning/Cs, Cs-F), "C" indicates Cs only. The cathode was recesiated when the cathode charge limit for a fully illuminated cathode dropped to the charge required for machine operations. During the first activation cycle, the operating charge was being slowly increased. For the second cycle, the nominal operating charge (see Table 6) was achieved.
15. Quantum efficiency (833 nm and 120 kV) for the second activation cycle during the 1993 SLC run. There were 29 recesiations during this period. Day 0 was April 22, 1993.
16. P_e and QE for the 100-nm strained-lattice cathode (cathode IV in Table 4) as a function of λ, measured at room temperature with the CTS Mott. At room temperature, the band gap for unstrained GaAs decreases with temperature by ~0.4 meV/°C. Thus at the operating temperature of the cathode, 0°C, the polarization peak is shifted by ~5 nm to ~845 nm.
17. P_e at the photocathode electron source as a function of QE measured with the Cathode Test System Mott and the E-143 End Station A Møller [120]. The statistical (systematic) errors are indicated by the inner (outer) error bars. The systematic errors for each polarimeter are 100% correlated.

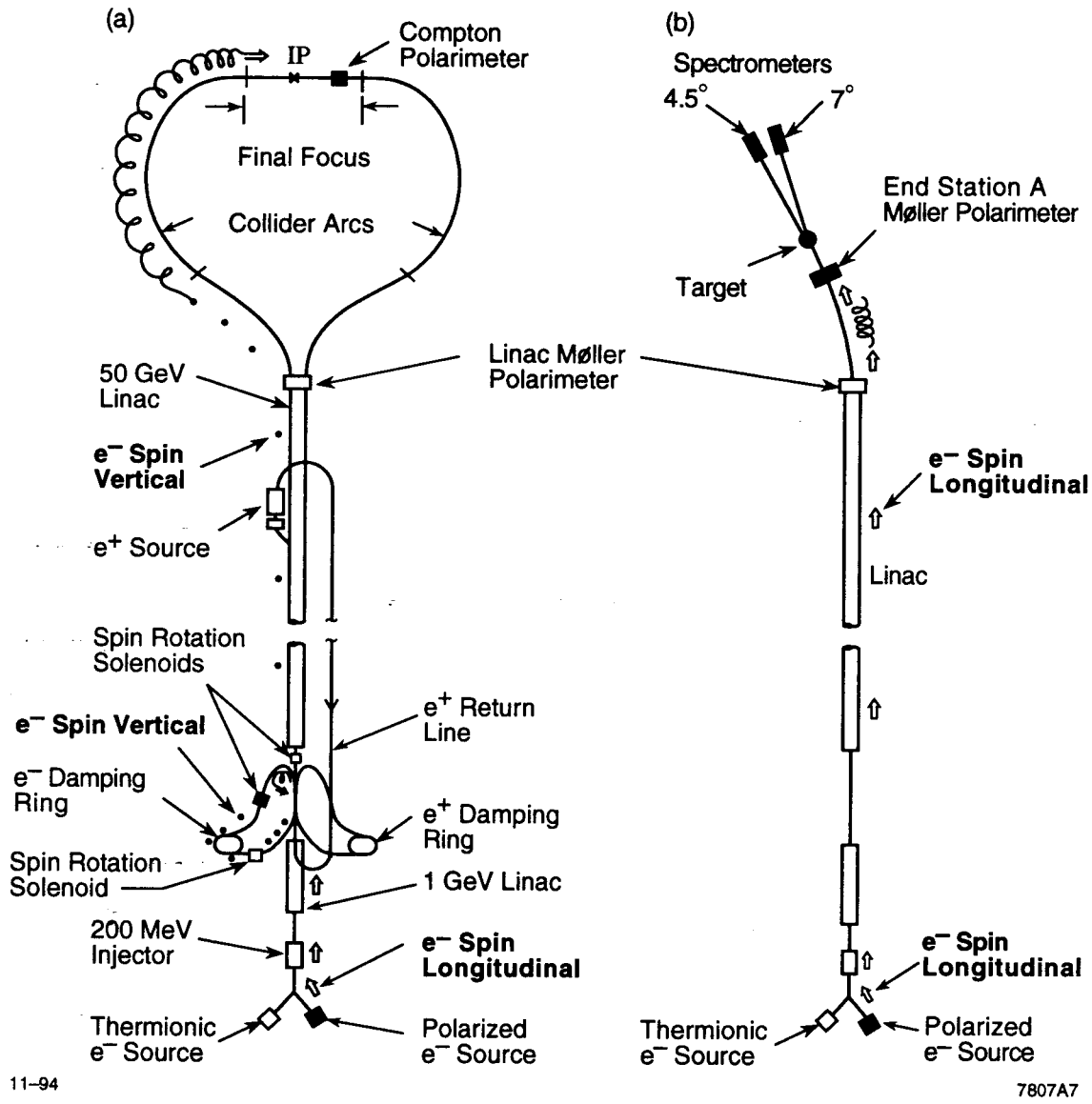
(a)
IP
Compton Polarimeter
Final Focus
Collider Arcs
50 GeV Linac
e⁻ Spin Vertical
e⁺ Source
Spin Rotation Solenoids
e⁻ Spin Vertical
e⁻ Damping Ring
Spin Rotation Solenoid
200 MeV Injector
Thermionic e⁻ Source
e⁺ Return Line
e⁺ Damping Ring
1 GeV Linac
e⁻ Spin Longitudinal
Polarized e⁻ Source
11-94
(b)
Spectrometers
4.5°
7°
End Station A Møller Polarimeter
Target
Linac Møller Polarimeter
e⁻ Spin Longitudinal
Linac
e⁻ Spin Longitudinal
Thermionic e⁻ Source
Polarized e⁻ Source
7807A7

Fig. 1

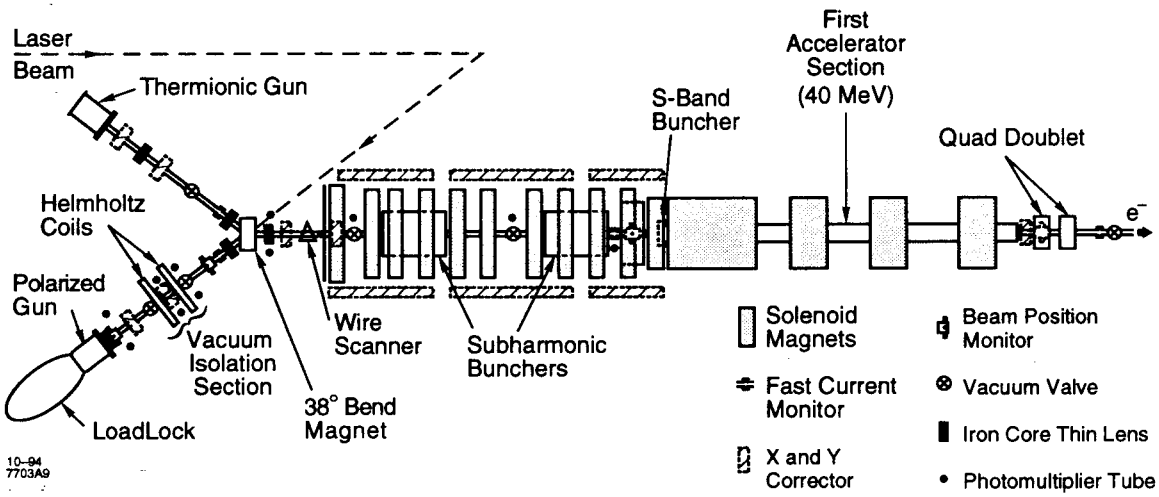
Laser
Beam
Thermionic Gun
Helmholtz
Coils
Polarized
Gun
Vacuum
Isolation
Section
LoadLock
38° Bend
Magnet
Wire
Scanner
Subharmonic
Bunchers
S-Band
Buncher
First
Accelerator
Section
(40 MeV)
Quad Doublet
e⁻
Solenoid
Magnets
Fast Current
Monitor
X and Y
Corrector
Beam Position
Monitor
Vacuum Valve
Iron Core Thin Lens
Photomultiplier Tube
10-94
7703A9

Fig. 2

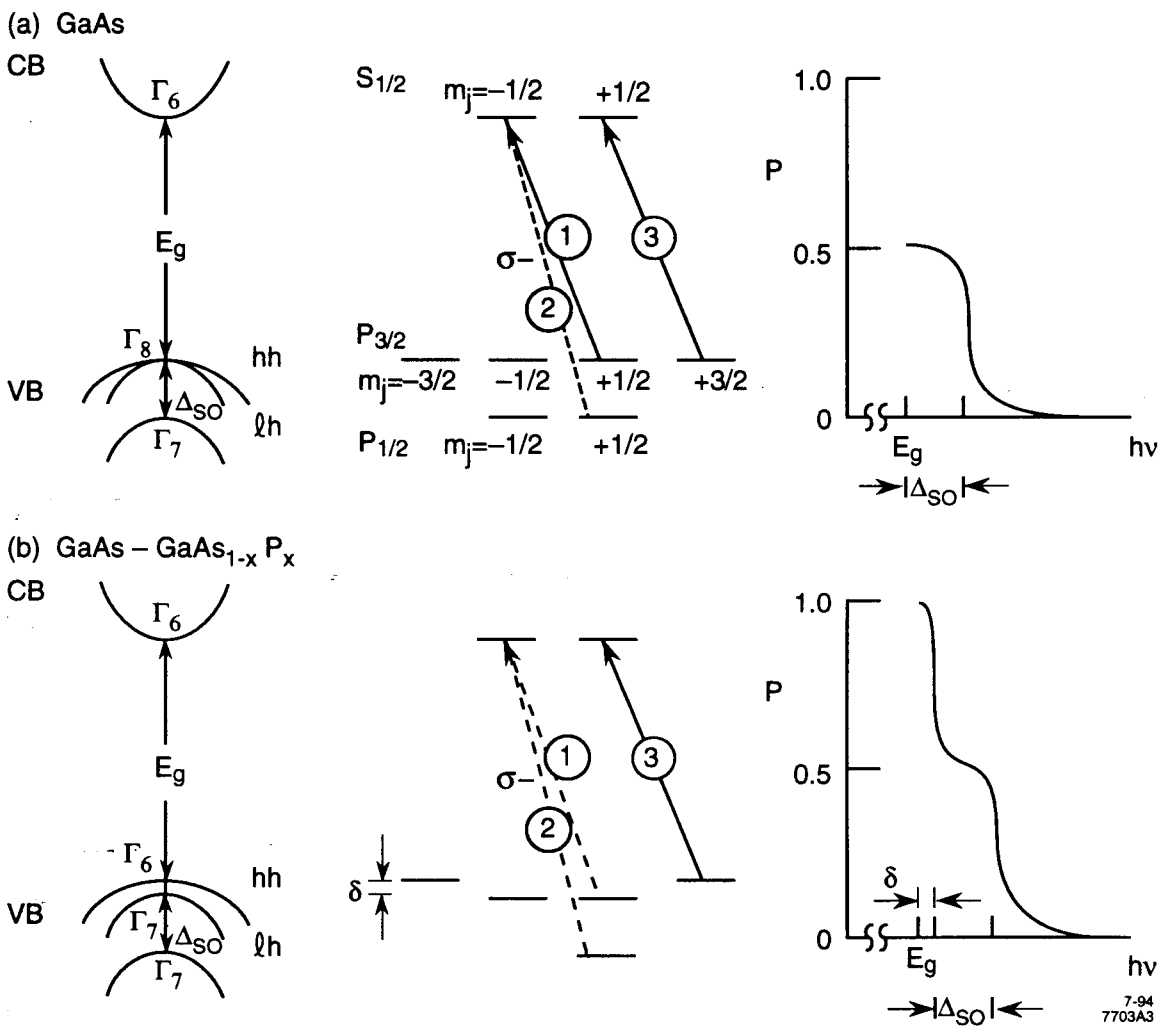
(a) GaAs
CB
Γ6
Eg
Γ8
hh
VB
Δso
ℓh
Γ7
S1/2
mj=−1/2
+1/2
σ−
1
2
3
P3/2
mj=−3/2
−1/2
+1/2
+3/2
P1/2
mj=−1/2
+1/2
1.0
P
0.5
0
Eg
hν
Δso
(b) GaAs – GaAs1-x Px
CB
Γ6
Eg
Γ6
hh
VB
Γ7
Δso
ℓh
Γ7
δ
σ−
1
2
3
1.0
P
0.5
0
δ
Eg
hν
Δso
7-94
7703A3

Fig. 3

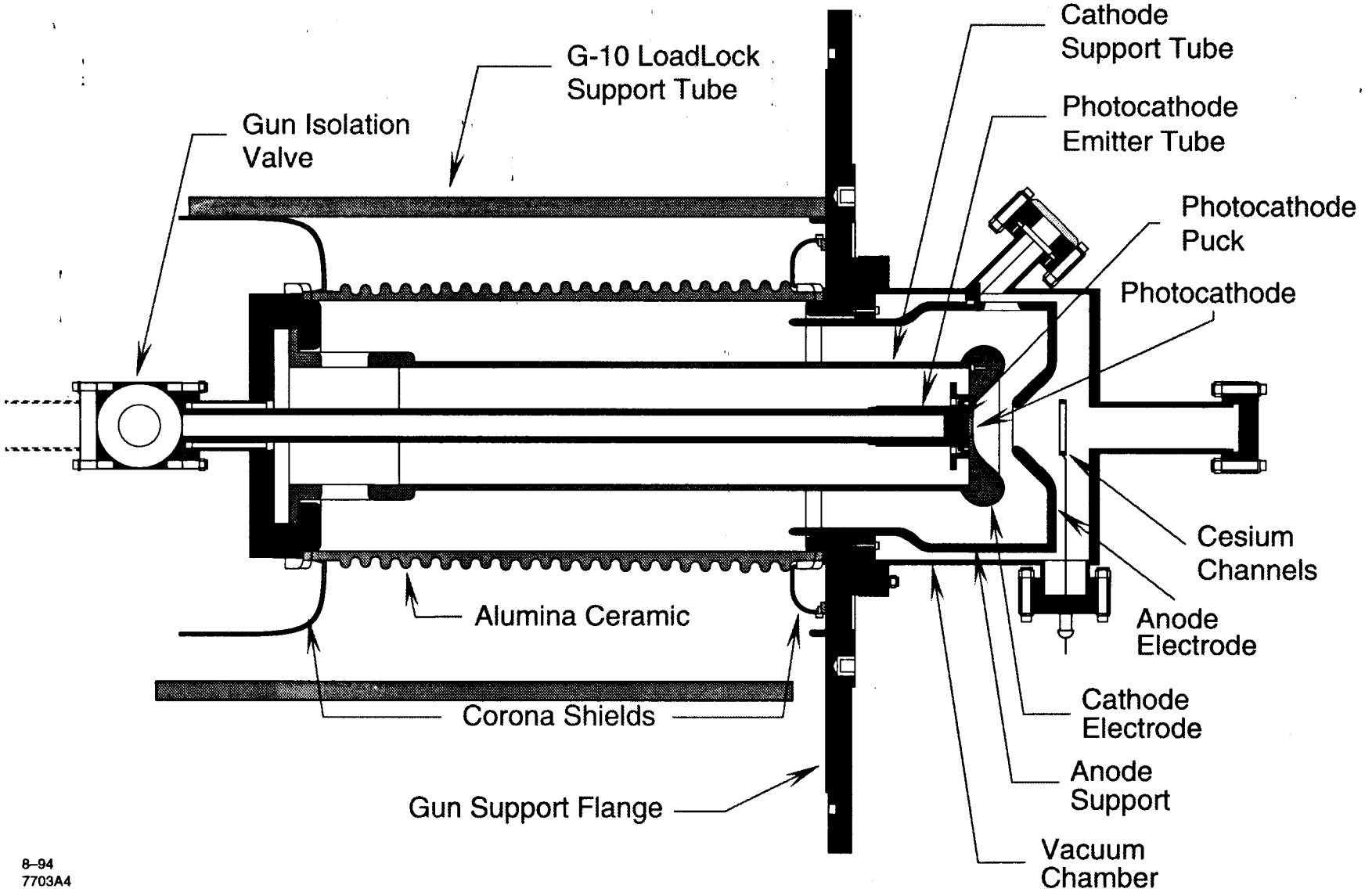
Cathode
Support Tube
G-10 LoadLock
Support Tube
Photocathode
Emitter Tube
Gun Isolation
Valve
Photocathode
Puck
Photocathode
Cesium
Channels
Alumina Ceramic
Anode
Electrode
Cathode
Electrode
Corona Shields
Anode
Support
Gun Support Flange
Vacuum
Chamber
8-94
7703A4

Fig. 4

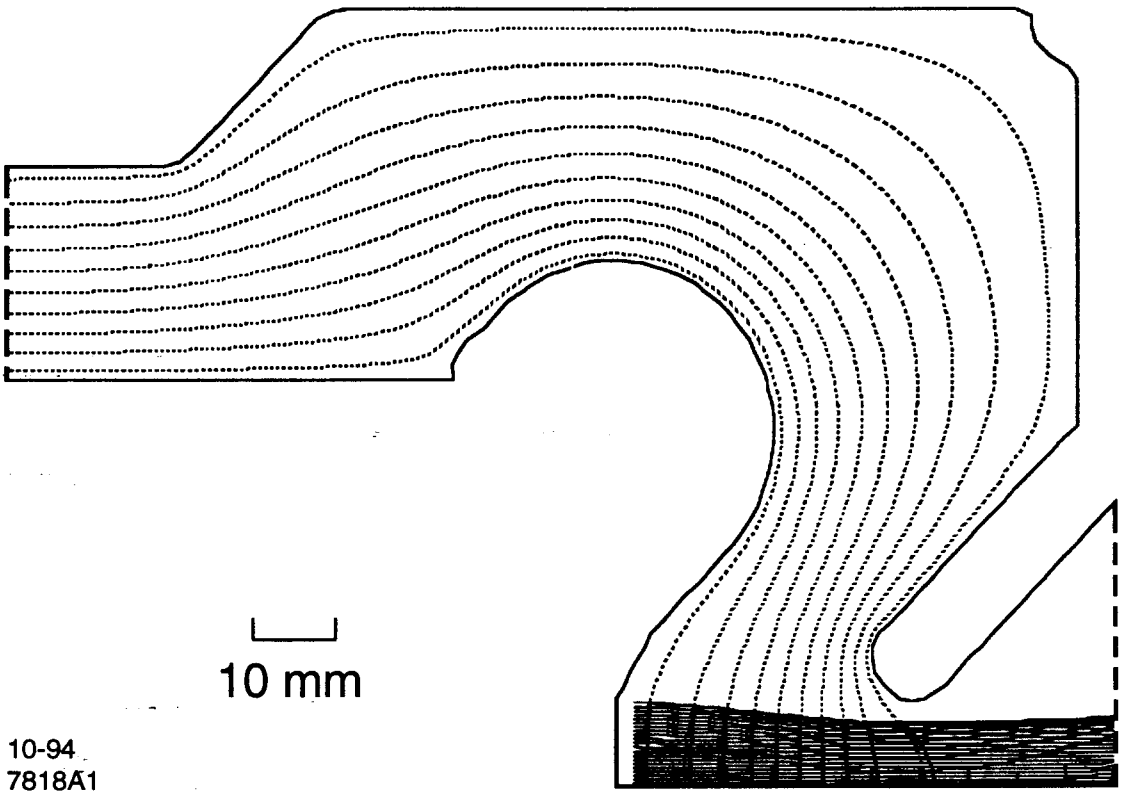

Fig. 5

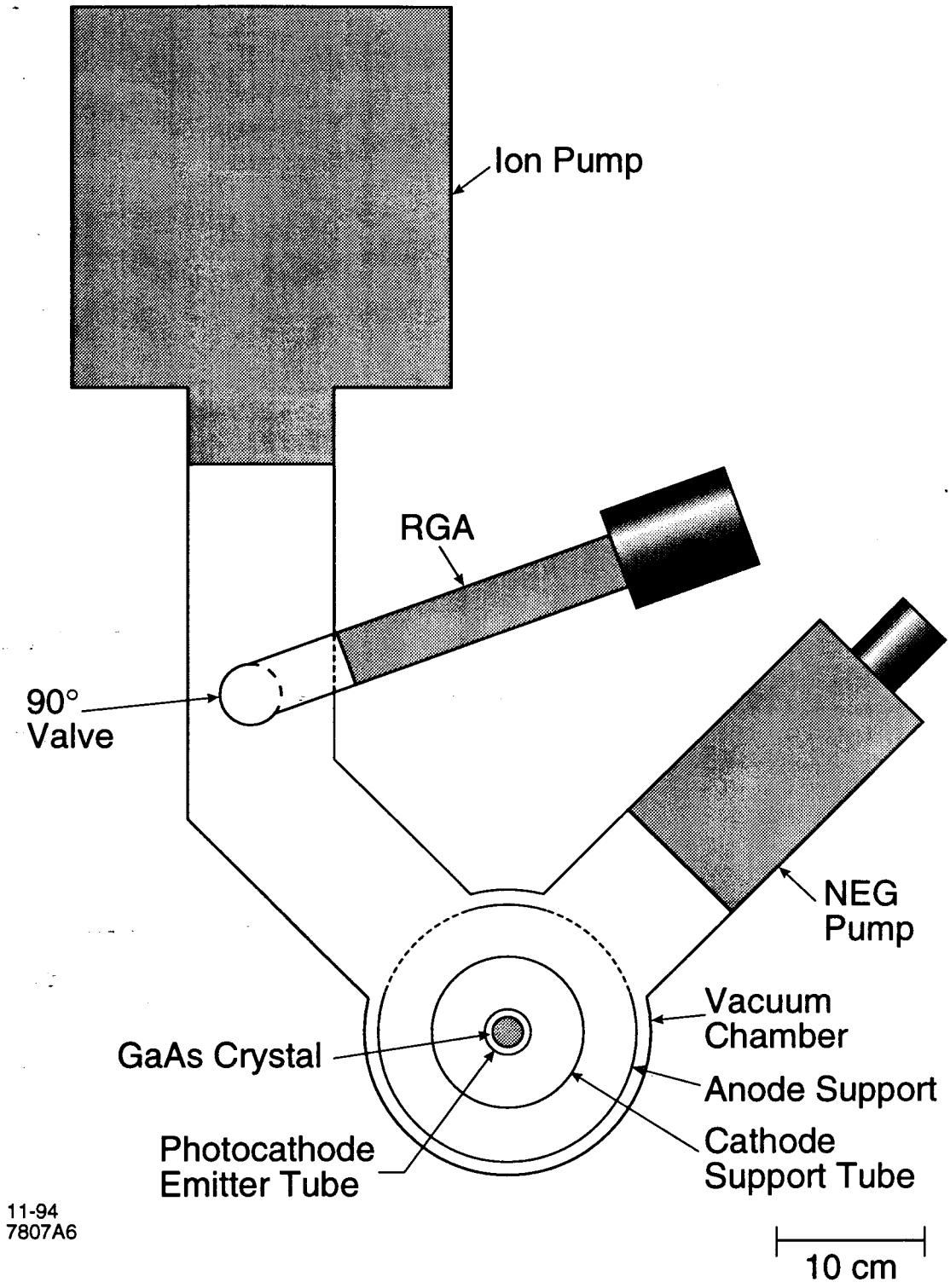
Ion Pump
RGA
90°
Valve
NEG
Pump
Vacuum
Chamber
GaAs Crystal
Anode Support
Photocathode
Emitter Tube
Cathode
Support Tube
11-94
7807A6
10 cm

Fig. 6

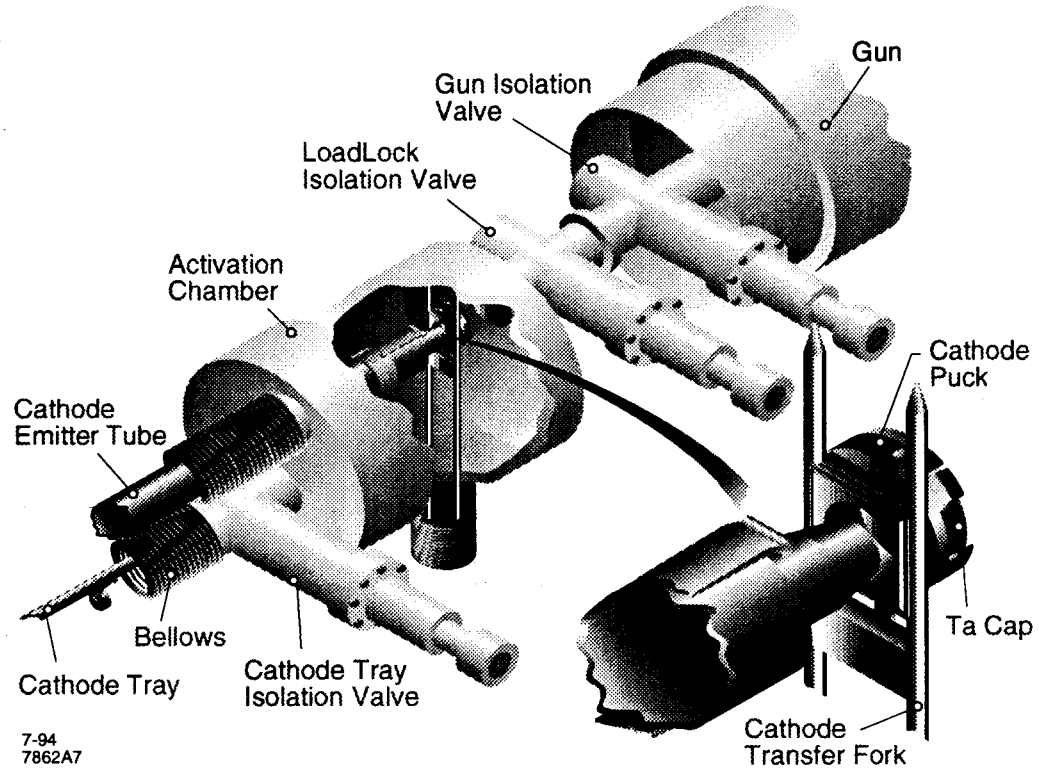
Gun
Gun Isolation Valve
LoadLock Isolation Valve
Activation Chamber
Cathode Puck
Cathode Emitter Tube
Ta Cap
Bellows
Cathode Tray
Cathode Tray Isolation Valve
Cathode Transfer Fork
7-94
7862A7

Fig. 7

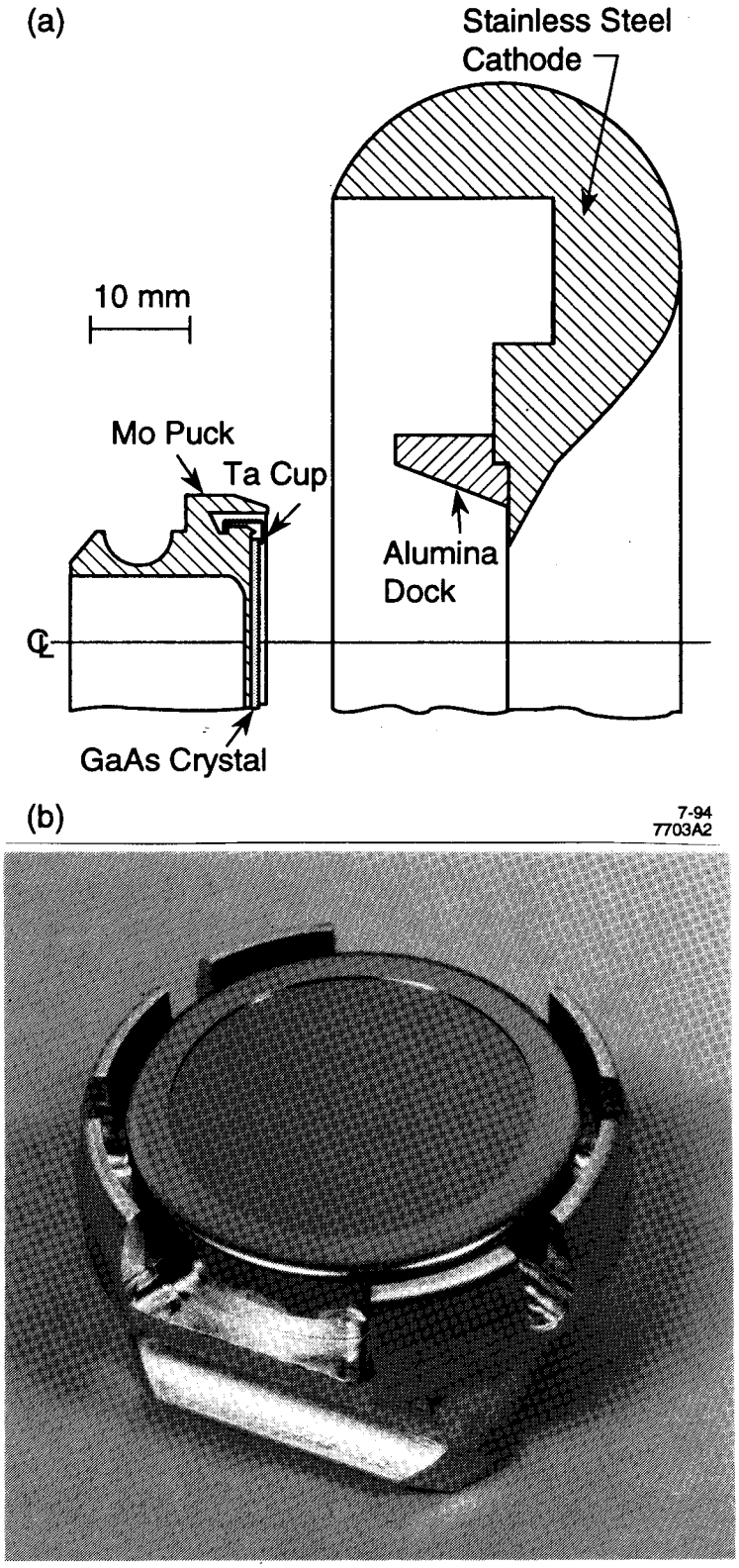
(a)
Stainless Steel
Cathode
10 mm
Mo Puck
Ta Cup
Alumina
Dock
GaAs Crystal
(b)
7-94
7703A2

Fig. 8

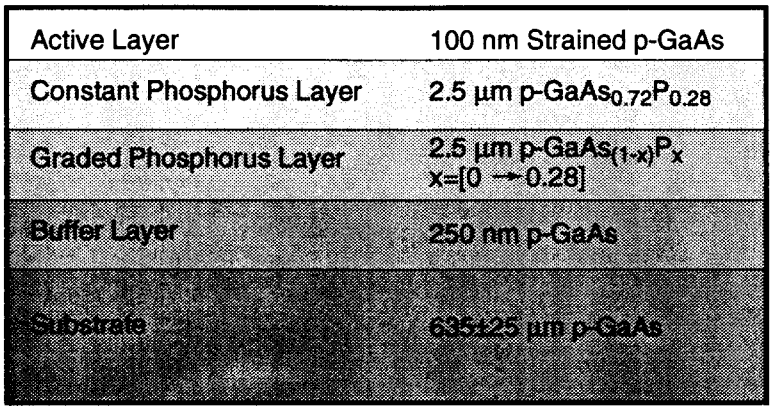
Active Layer
100 nm Strained p-GaAs
Constant Phosphorus Layer
2.5 µm p-GaAs0.72P0.28
Graded Phosphorus Layer
2.5 µm p-GaAs(1-x)Px
x=[0 → 0.28]
Buffer Layer
250 nm p-GaAs
Substrate
635±25 µm p-GaAs
1-95
7862A9

Fig. 9

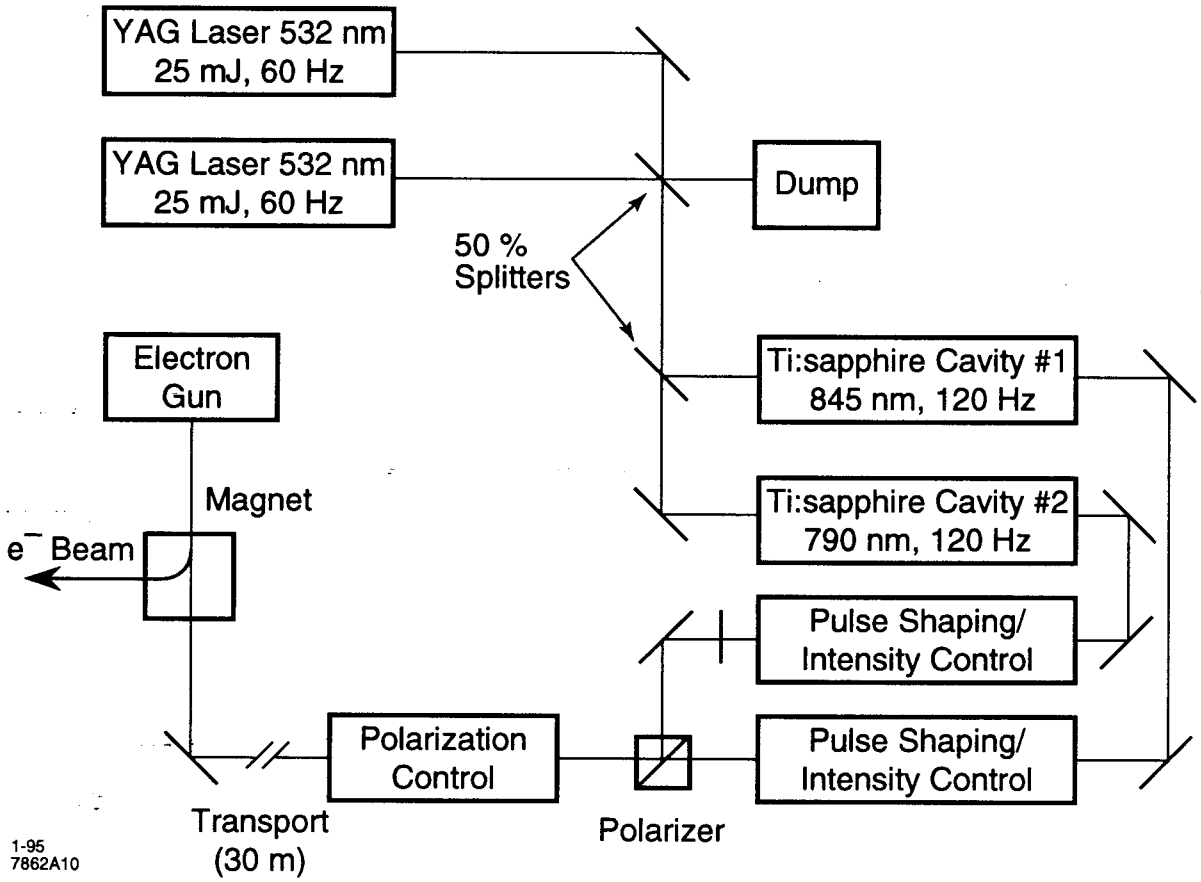
YAG Laser 532 nm
25 mJ, 60 Hz
YAG Laser 532 nm
25 mJ, 60 Hz
Dump
50 %
Splitters
Electron
Gun
Ti:sapphire Cavity #1
845 nm, 120 Hz
Magnet
e⁻ Beam
Ti:sapphire Cavity #2
790 nm, 120 Hz
Pulse Shaping/
Intensity Control
Polarization
Control
Pulse Shaping/
Intensity Control
Transport
(30 m)
Polarizer
1-95
7862A10

Fig. 10

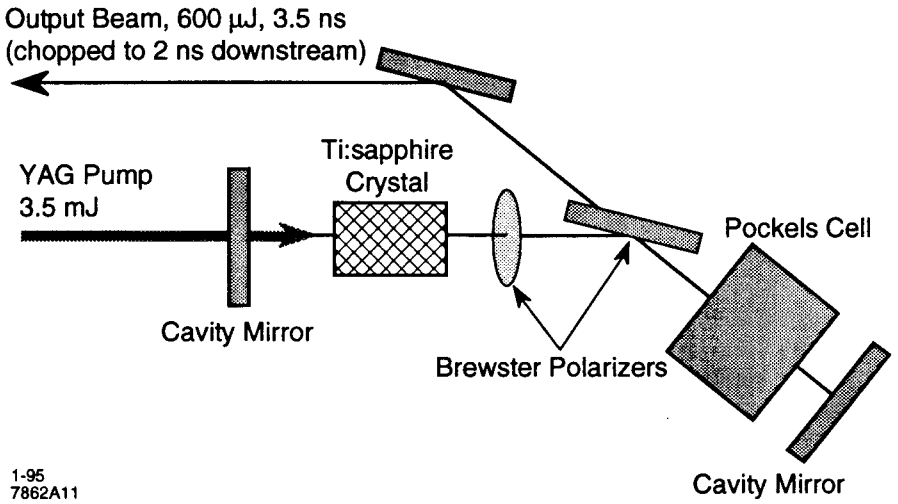
Output Beam, 600 μJ, 3.5 ns
(chopped to 2 ns downstream)
YAG Pump
3.5 mJ
Ti:sapphire
Crystal
Pockels Cell
Cavity Mirror
Brewster Polarizers
Cavity Mirror
1-95
7862A11

Fig. 11

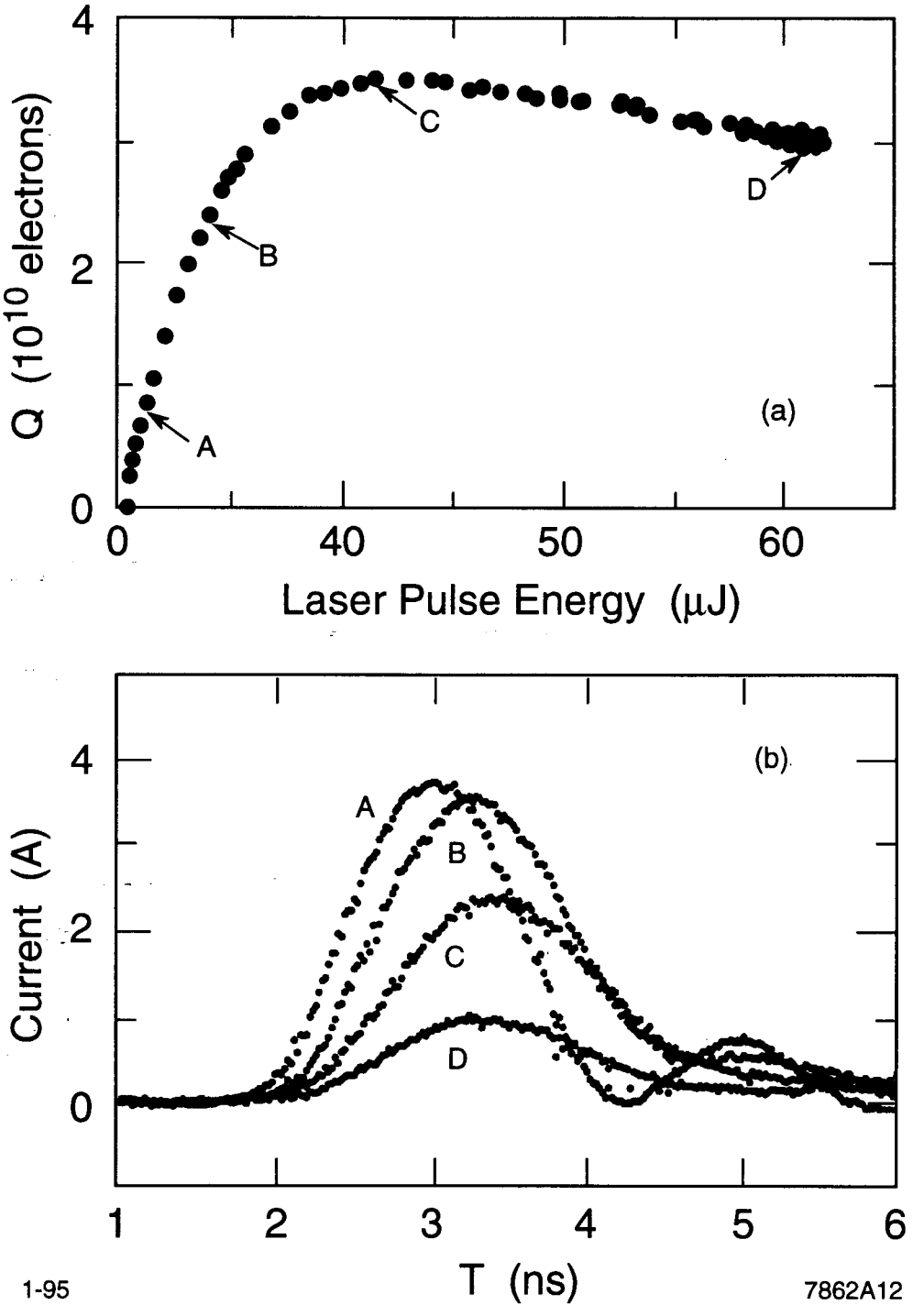
Q (10^{10} electrons)
Laser Pulse Energy (μJ)
(a)
A
B
C
D
Current (A)
T (ns)
(b)
1-95
7862A12

Fig. 12

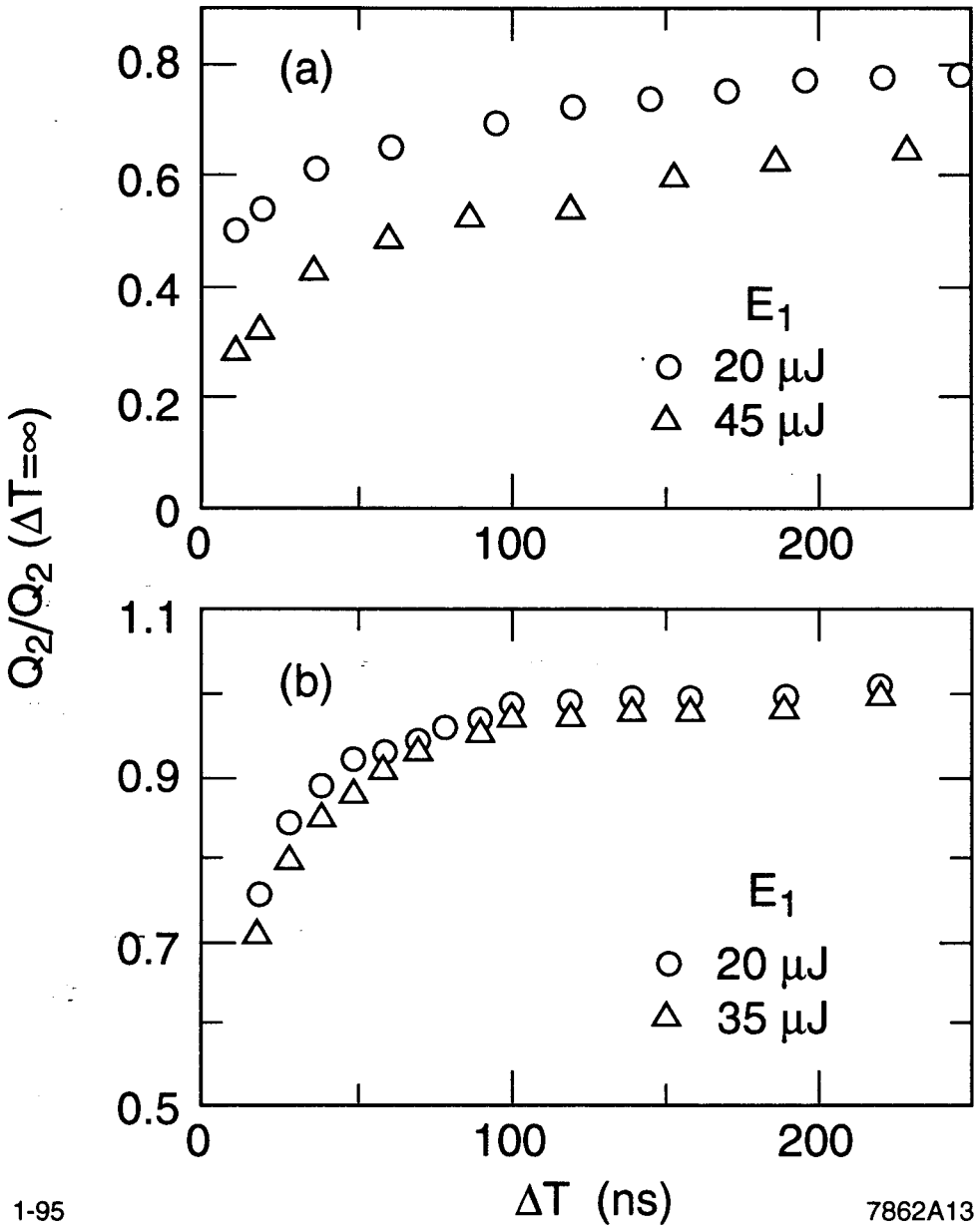
(a)
0.8
0.6
0.4
0.2
0
0
100
200
E1
20 μJ
45 μJ
(b)
1.1
0.9
0.7
0.5
0
100
200
E1
20 μJ
35 μJ
Q2/Q2 (ΔT=∞)
ΔT (ns)
1-95
7862A13

Fig. 13

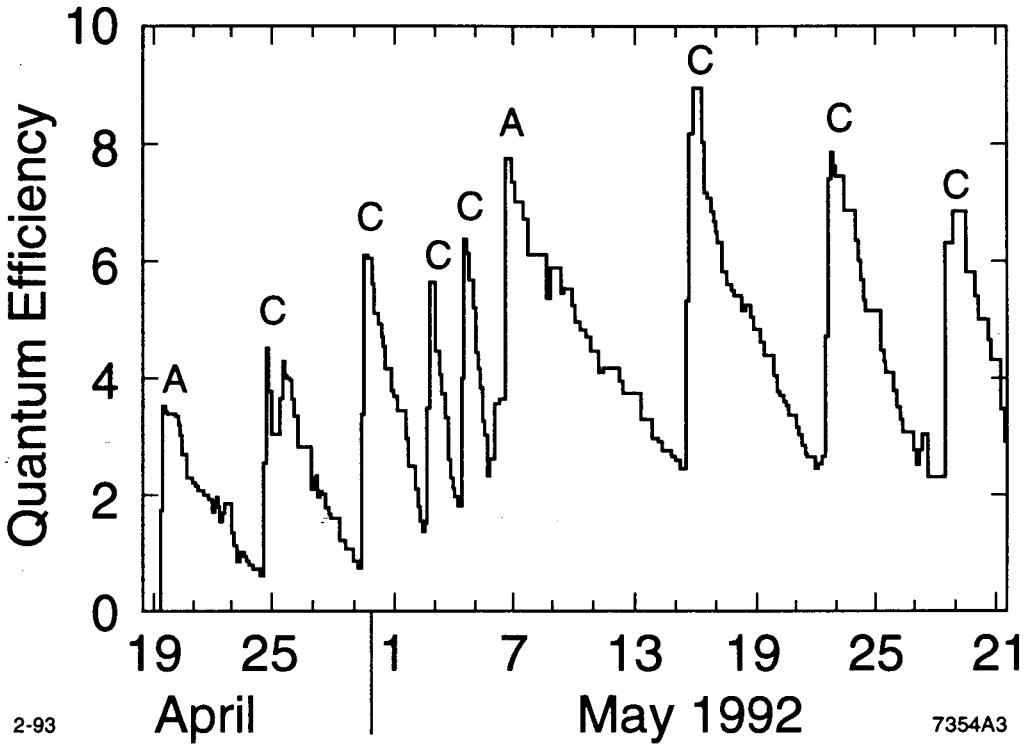
Quantum Efficiency
10
8
6
4
2
0
A
C
C
C
C
A
C
C
C
19
25
1
7
13
19
25
21
April
May 1992
2-93
7354A3

Fig. 14

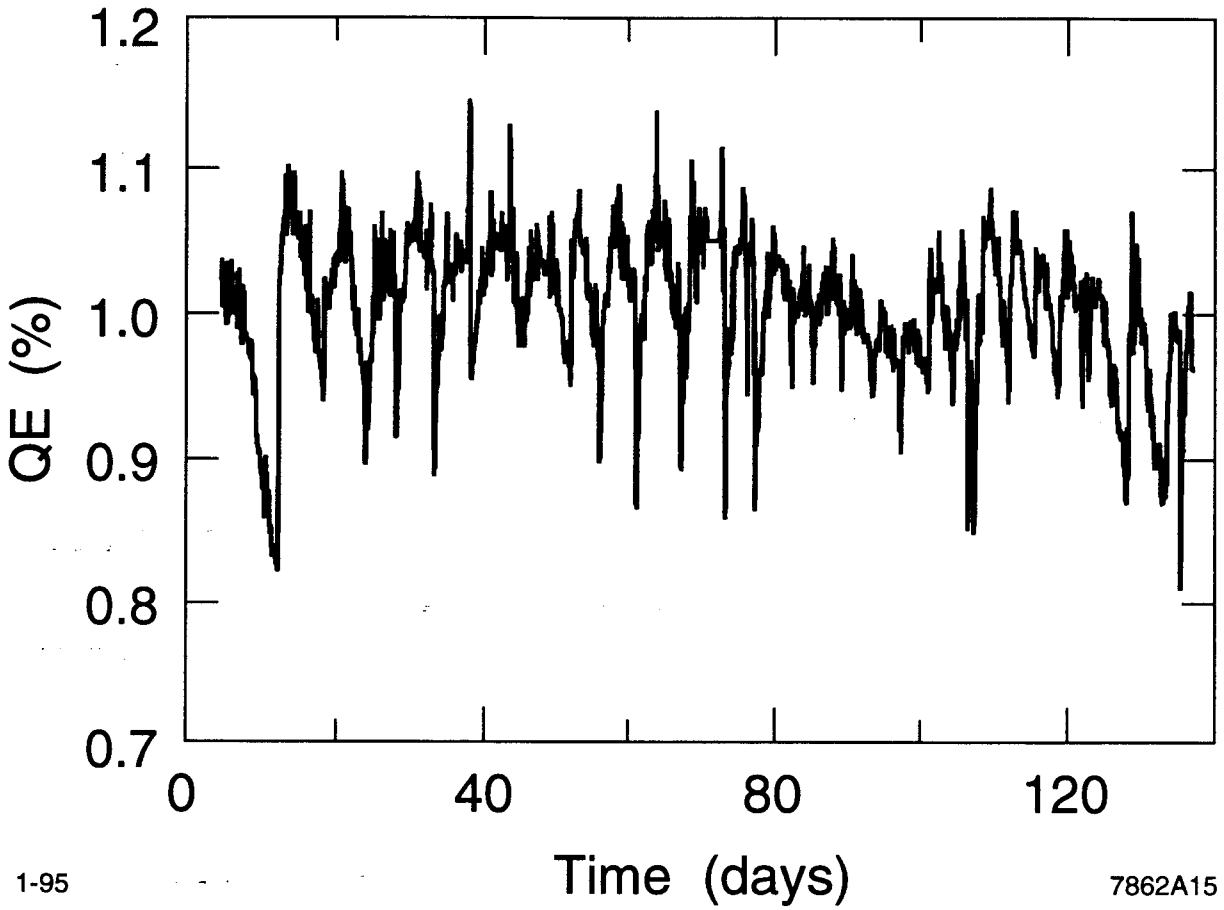

Fig. 15

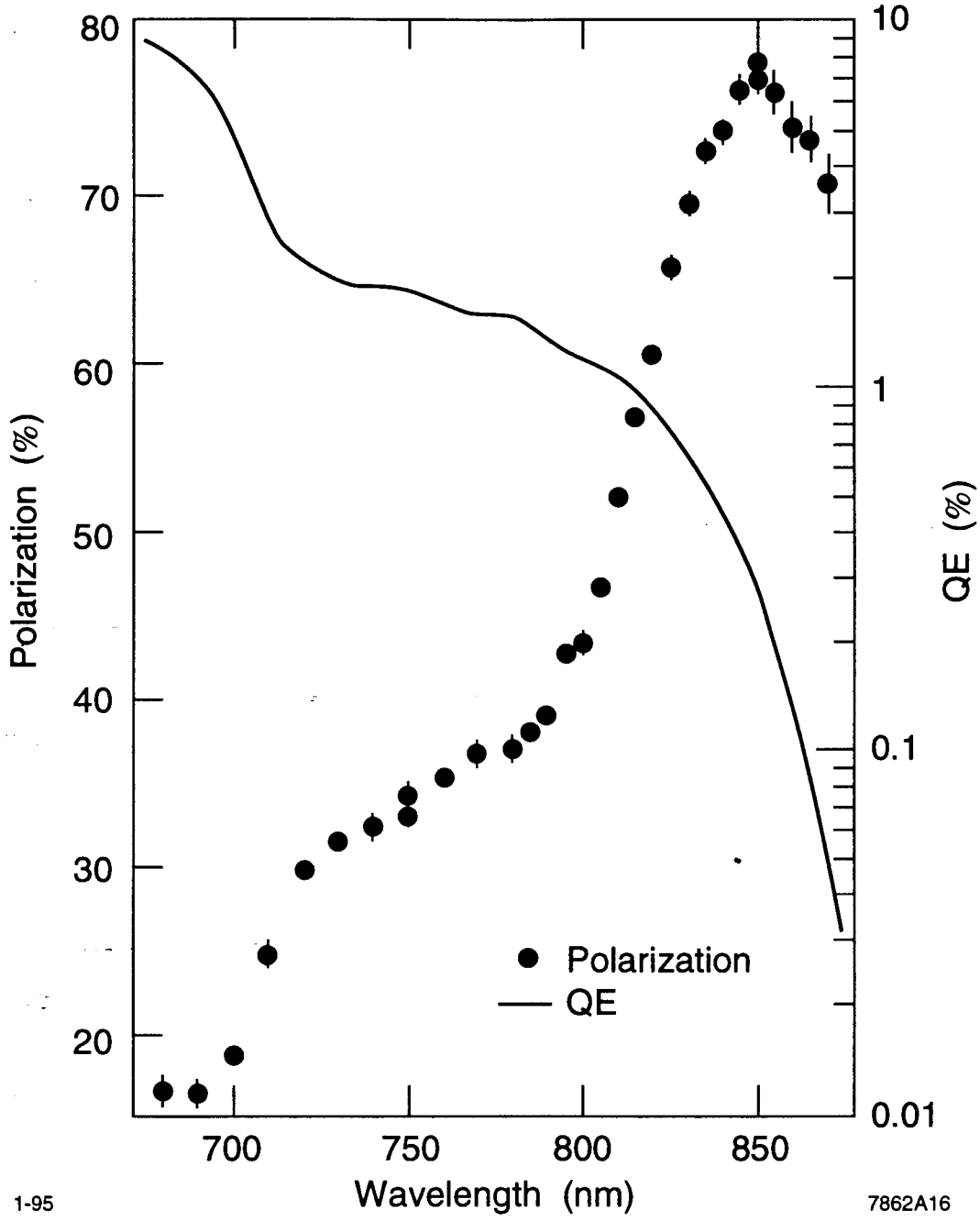
80
70
60
50
40
30
20
Polarization (%)
10
1
0.1
0.01
QE (%)
700
750
800
850
Wavelength (nm)
Polarization
QE
1-95
7862A16

Fig. 16

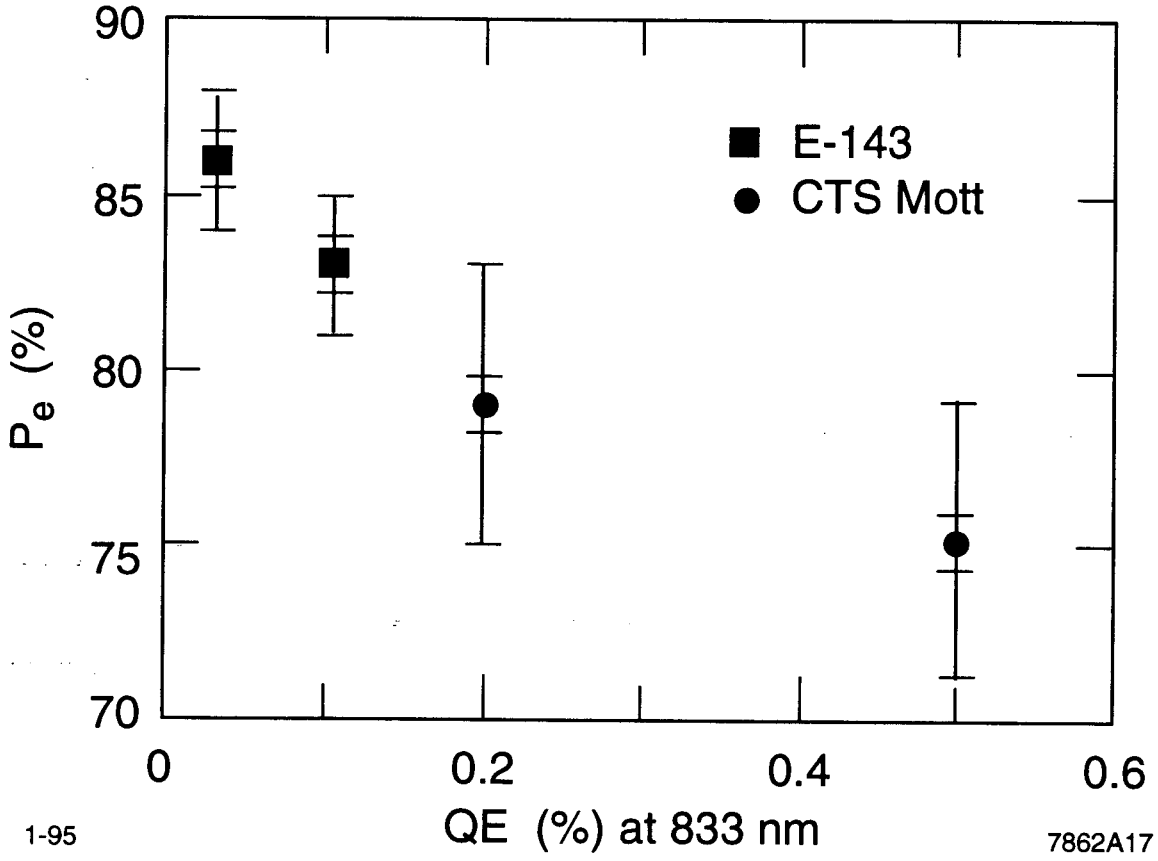

Fig. 17